

## Response to Editor's comments (Manuscript Ref. NO.: acp-2017-120)

We appreciate the editor for the thoughtful comments and guidance. The manuscript has been carefully checking for the errors and the consistency in model description. The responses to the comment are shown below.

**1) Referee #1, Comment 1:** The partitioning between the gas and condensed phase are treated in a similar way, despite being fundamentally different in nature. For a solid surface, the adsorption and desorption processes do follow a different formalism, typically through a Langmuir-Hinshelwood formalism which takes into account a given number of adsorption sites. The consequences is that adsorption decreases with time or increasing concentration, while here it is simulated in a constant way with time. how can you justify such an assumption? Also products such as sulfate are probably staying on the surface, thereby also using adsorption sites i.e., poisoning the surface. How would your model change if you implement such time/concentration dependence?

**Previous Response:** We assumed that the gas-particle partitioning onto dust is operated by an absorption process (Eq. 7) by several reasons (see section 3.2.1). First, unlike pure metal oxide which is governed by the adsorptive partitioning, the composition of authentic mineral dust such as Arizona Test Dust (ATD) is complex. The fresh ATD contains inorganic salts that are hygroscopic and form the water film above efflorescence relative humidity or deliquescence relative humidity. Second, the partitioning process is dynamic due to the formation of various hygroscopic salts of sulfate and nitrate due to the reaction of alkaline carbonates and metal oxides with inorganic acids (sulfuric acid and nitric acid). Third, the sulfate formation in our study increased as increasing humidity due to the dissolution of tracers into the water layer (see section 3.2.1). If partitioning is processed by the adsorptive mode, water molecules compete for the site with tracers and reduce partitioning of tracers (Cwierny et al., 2008). The amount of the surface water on dust particles, which was measured using FTIR (submitted in the other journal), was multi-layered.

**Editor:** It seems to me that the only change in response to this comment was that you replaced all 'adsorption' by 'absorption' in the manuscript. However, this raises more questions than it adds to clarification. You argue that the hygroscopic fraction of the dust forms an aqueous phase where then the chemical processing in the 'dust phase' occurs. Thus, the extent of this processing will depend on the mass (volume) of the hygroscopic dust material. It is not clear to me why parameters such as the absorption rate constants (e.g.  $R_5$  and Equation 5) can be used that relate to a particle surface ( $m^{-2}$ ) and not to a (partial) particle volume. This should be clarified throughout the manuscript. The text should be carefully checked for consistency (e.g. p. 15, l. 10 'adsorption-desorption') and conclusions should be refined (e.g. why is BET surface area needed (p. 20, l. 26) if the hygroscopic material determines the reactions medium?)

**Response to Editor:** We agree with the Editor's view. In the revised manuscript, we use word "adsorption-desorption" for gas-dust partitioning of tracers (i.e., SO<sub>2</sub> or NO<sub>2</sub>). Unlike partitioning on pure metal oxide, gas-dust partitioning is processed on the multilayer coated dust with water molecules. In order to clarify this, the sentence was added into the revised manuscript and reads now, "The partitioning processes between the gas phase and multilayer coated dust were treated by the adsorption-desorption kinetic mechanism." (1<sup>st</sup> paragraph in Section 3). Please also see the 1<sup>st</sup> paragraph of Section 3.2.1 Gas-dust particle partitioning.

**2) Referee #1, Comment 4:** Too many rate constants are estimated without any justification. Please justify and explain your estimations.

**Response:** Most of the rate constants shown in Table 3 were estimated using the indoor chamber data obtained in the previous study (Park and Jang, 2016). The rate constants of R10 (electron-hole production) and R11 (recombination of electron-hole) in the manuscript is estimated using Eq. 10 (photoactivation rate, JATD) in the manuscript (Section 3.2.3). The rate constant of R13 (reaction of SO<sub>2</sub> with dust-phase OH radicals) is set to the same reaction rate constant for the reaction of SO<sub>2</sub> with OH radicals in gas phase. Without sunlight, autoxidation of SO<sub>2</sub> (R9) is dominant in dust phase and its rate constant was obtained from indoor chamber data under various humidity conditions (Exp. D1-D3 in Table 1). With sunlight, the photochemical reaction is the major source for sulfate production. Using the same approach with autoxidation, the rate constant of R12 was estimated under different humidity conditions. Also, the rate constants of R14 (heterogeneous autoxidation of SO<sub>2</sub> in the presence of ozone) and R15 (heterogeneous oxidation of O<sub>3</sub>) were estimated using experiments D4 and L5 in Table 1, respectively. The rate constants of R18 (heterogeneous autoxidation of NO<sub>2</sub>) and R19 (heterogeneous photocatalytic oxidation of NO<sub>2</sub>) were estimated using experiments D5 and L7 in Table 1, respectively.

**Editor:** In my opinion, your response is neither a justification nor an explanation why so many rate constants were estimated. (a) Please add a more detailed discussion of uncertainties and background on these constants in order to fulfill the reviewer's inquiry. (b) Also, I noticed that e.g.  $K_{d,SO_2}$  is used for dry particles – how can this be justified?

**Response to Editor:**

(a) Thank you much for the editor's comment on uncertainties of model parameter and the prediction of sulfate. The third paragraph in Section 5 and Figure S7 were revised to illustrate the uncertainty in major model parameters ( $[H^+]$ ,  $F_{water}$ ,  $K_{d,SO_2}$ ,  $k_{auto}$  and  $k_{OH,O_2}$ ) and the formation of sulfate ( $[SO_4^{2-}]_T$ ). Please also notice the figure caption in Figure S7 for the detailed explanation.

The rate constants of heterogeneous photooxidation reactions of SO<sub>2</sub> and NO<sub>2</sub> on airborne mineral dust were unknown. In order to obtain the rate constants for the dust phase chemistry, we ran our model using the indoor data reported by Park and Jang (2016). In the 2<sup>nd</sup> paragraph of Section "3

AMAR model description”, we summarized the source data used for processing major model parameters.

“The rate constants associated with various reaction mechanisms in the AMAR model were determined by simulating pre-existing indoor chamber data obtained from controlled experimental conditions (Park and Jang, 2016). For example, the rate constant ( $k_{auto}$ ,  $s^{-1}$ ) for  $SO_2$  autoxidation is semiempirically determined by fitting the predicted concentration of sulfate to the experimental data D1 in Table 1. The gas–dust partitioning constant ( $K_{d,SO_2}$ , Sect. 3.2.1) of  $SO_2$  is dependent of temperature, aerosol water content, and acidity.  $K_{d,SO_2}$  values were semiempirically determined using data D1-D3 (three different RHs) and the literature parameters related to the effect of temperature and acidity on  $K_{d,SO_2}$ . The rate constant ( $k_{photo}$ ,  $cm^3 \text{ molecule}^{-1} s^{-1}$ ) for sulfate formation by photocatalytic reactions is semiempirically determined using data L1-L3 (three different RHs) in Table 1. In the presence of ozone,  $k_{auto}$  and  $k_{photo}$  are determined using data D4 and L4, respectively.”

(b) The value of  $K_{d,SO_2}$  at 20% RH was obtained from literature data (Adams et al. 2005; Huang et al. 2015). In order to estimate  $K_{d,SO_2}$  at different RH, data D1-D3 in Table 1 (three different RHs) were used to estimate the effects of humidity on the gas-dust partitioning process. Thus,  $K_{d,SO_2}$  is a function of RH.

**3) Referee #2, Comment 2:** In addition to react with  $SO_2$  and  $NO_2$ , OH radicals produced on the surface of particles under UV conditions can undergo heterogeneous reaction with particles as well as self-reactions, resulting in the significant decrease of OH radicals participate in the oxidation of  $SO_2$  and  $NO_2$ , and subsequently overestimating sulfate and nitrate formation in the model. Furthermore, in addition to compete OH radicals with  $SO_2$ , the presence of  $NO_2$  can also react with  $SO_2$  on the surface of particles to promote sulfate formation at high RHs as like in aqueous phase. However, these mechanisms were not considered in dust phase in the model (Table S1).

**Response:** In our model, the apparent rate constant of the formation of the dust-phase OH radicals is estimated using indoor chamber data. The synergistic effect of  $NO_2$  on sulfate formation under UV light is explained by the HONO production through the reaction of  $NO_2$  with electrons or holes in dust phase (R16). HONO will then be decomposed via photolysis to form OH radicals (R17).

**Editor:** The reviewer’s concern of missing reactions in your mechanism is well justified. How would the recombination of OH or their loss on particle surfaces affect your results? Please add a discussion about what it is known about such processes and to what extent they may compete with other processes in your system.

**Response to Editor:** In current our knowledge, the amount and the type of conductive metal oxides in ATD particles are unclear. In our model, the formation of OH radicals on dust is operated using apparent rate constants for the formation and decay of electron-hole (R10 and R11). The mechanistic role of the catalytic formation of the electron-hole pair (R10) and their

recombination (R11) can compensate the formation and the self-reaction of OH radicals (Section 3.2.3).

#### **4) Difference between dust chemistry and aqueous phase chemistry**

**Editor:** Related to the comment above, I do not understand the fundamental difference between the aqueous phase chemistry (Section 3.1.3) and dust chemistry (Section 3.2). Both are reactions that occur in a bulk aqueous phase and thus mechanistically they should be treated equally (even though different chemical reactions occur). Please justify the differentiation into two types of processes. It should be stated throughout the manuscript that the ‘dust phase’ is also technically an aqueous phase

**Response to Editor:** Please also find the response to editor’s comment 1. The aqueous phase reaction is processed in a bulk phase while dust chemistry occurs in the multilayer comprising electrolytes and water on dust surfaces. Hence, the estimation of the water content on dust surfaces, which is influenced by hygroscopic properties of dust surfaces, temperature, and acidity, is essential as discussed in Section 3.2.1. The water content on dust surfaces is also dependent of the amount of dust (relevant to the surface area) and dust compositions.

#### **5) Use of Henry’s law constants**

**a)** What is the ionic strength and/or acidity of the aqueous phases? Is the application of Henry’s law constants (for ideal solutions) justified? If not, how does this affect the results and the possibility of extrapolation of the derived rate constants to other conditions?

**Response to Editor:** In AMAR, aerosol acidity ( $[H^+]$ , mol L<sup>-1</sup>) is estimated at each time step by E-AIM II (Clegg et al., 1998; Wexler and Clegg, 2002; Clegg and Wexler, 2011) corrected for the ammonia rich condition (Li and Jang, 2012; Li et al., 2015; Beardsley and Jang, 2016) as a function of inorganic composition measured by PILS-IC (Section 3.1.3).

For the highly concentrated electrolyte aerosol, the deviation of the compound’s solubility predicted using Henry’s constants from the actual solubility would be varied depending upon the chemical structure. In the current knowledge, we do not know the actual Henry’s constant of each species in the highly concentrated electrolyte solution. For aqueous phase reactions (no dust), Henry’s constants that are reported in the modeling paper by Liang and Jacobson (1999) were applied to the AMAR model. Although this implementation can be potentially problematic to predict sulfate production, our model simulation reasonably predicted outdoor chamber data (Figure 3(a) in Section 4.1)

For dust heterogeneous chemistry, Henry’s constants of various tracers were used to scale their gas-dust partitioning coefficient based on the known value for SO<sub>2</sub> on ATD dust particles (Section 3.2.1). For example, the literature value for the gas-ATD partitioning coefficient of SO<sub>2</sub> was 1.3 m<sup>3</sup> m<sup>-2</sup> at 20% RH. The gas-ATD partitioning coefficient of SO<sub>2</sub> is much greater than Henry’s constant by several orders (10<sup>5</sup>) when the same unit is applied to both constants (m<sup>3</sup>/μg). The scaling of the gas-ATD partitioning coefficients of the tracers of this study using Henry’s

constants may cause some inaccuracy in the estimation of the concentration of adsorbed tracers due to the difference in the activity coefficient of each compound in different media (dust surface vs. dilute aqueous phase). As shown in Figure 3 (Section 4.1), the sulfate production in the presence of ATD particles reasonably accorded with chamber data.

**b)** Is the pH sufficiently low that the uptake of SO<sub>2</sub> can be indeed solely described by the physical Henry's law constant  $K_{H,SO_2}$ ? This can be only applied if the solution is sufficiently acidic and no dissociation occurs; otherwise the effective Henry's law constant including dissociation should be included. Please justify.

**Response to Editor:** As shown in Eq. (7), the impact of aerosol acidity on the gas-dust partitioning of SO<sub>2</sub> is treated in the model. When pH is low, the uptake of SO<sub>2</sub> is still influenced by humidity and aerosol compositions for both aqueous phase reactions and dust heterogeneous chemistry. As shown in Figure 5, the humidity conditions can significantly influence sulfate formation due to the higher uptake of SO<sub>2</sub> at the higher RH. In general, aerosol acidity has a compounding effect because the higher acidity can reduce the solubility of SO<sub>2</sub> (Eq. (7)) but increase hygroscopic property of aerosol. For aqueous phase reactions, we included the uptake process and acid dissociation reactions for HO<sub>2</sub>, HCOOH, HONO and HCHO (acid dissociation reactions in Table S1). In addition to reactions of inorganic species, the influence of organic species (i.e., HCOOH, HCHO, and CH<sub>3</sub>CHO) on dust heterogeneous chemistry needs to be investigated in the future (last paragraph in Section 6).

## 6) Language

The whole manuscript should be carefully checked for proper use of English language. I list some rather unusual or unclear expressions below (line numbers refer to the marked-up manuscript that was attached to the response of the reviews)

p. 6, l. 10: 'calculated to mass absorbance' – is there a word missing (e.g. 'obtain')?

p. 9, l. 3: What is a 'carry over for sulfate'

p. 11, l. 11: 'numeric number' is redundant

Figure 2, y-axis should be 'Uptake coefficient'

**Response to Editor:** The errors were corrected. The manuscript has been thoroughly checked for grammars and spelling.

## Marked-up manuscript

### Modelling Atmospheric Mineral Aerosol Chemistry to Predict Heterogeneous Photooxidation of SO<sub>2</sub>

Zechen Yu, Myoseon Jang, and Jiyeon Park

5 P.O. Box 116450, Department of Environmental Engineering Sciences, Engineering School of Sustainable  
Infrastructure and Environment, University of Florida, Gainesville, FL, USA, 32611

Corresponding author: Myoseon Jang, mjang@ufl.edu

#### Abstract.

The photocatalytic ability of airborne mineral dust particles is known to heterogeneously promote  
10 SO<sub>2</sub> oxidation, but prediction of this phenomenon is not fully taken into account by current models. In this  
study, the Atmospheric Mineral Aerosol Reaction (AMAR) model was developed to capture the influence  
of air-suspended mineral dust particles on sulfate formation in various environments. In the model, SO<sub>2</sub>  
oxidation proceeds in three phases including the gas phase, the inorganic-salted aqueous phase (non-dust  
phase), and the dust phase. Dust chemistry is described as the ~~absorption~~adsorption-desorption kinetics  
15 ~~(gas-particle partitioning)~~ of SO<sub>2</sub> and NO<sub>x</sub>-~~(partitioning between the gas phase and the multilayer coated~~  
~~dust)~~. The reaction of ~~absorbed~~adsorbed SO<sub>2</sub> on dust particles occurs *via* two major paths: autooxidation of  
SO<sub>2</sub> in open air and photocatalytic mechanisms under UV light. The kinetic mechanism of autooxidation  
was first leveraged using controlled indoor chamber data in the presence of Arizona Test Dust (ATD)  
particles without UV light, and then extended to photochemistry. With UV light, SO<sub>2</sub> photooxidation was  
20 promoted by surface oxidants (OH radicals) that are generated *via* the photocatalysis of semiconducting  
metal oxides (electron-hole theory) of ATD particles. This photocatalytic rate constant was derived from  
the integration of the combinational product of the dust absorbance spectrum and wave-dependent actinic  
flux for the full range of wavelengths of the light source. The predicted concentrations of sulfate and nitrate  
using the AMAR model agreed well with outdoor chamber data that were produced under natural sunlight.  
25 For seven consecutive hours of photooxidation of SO<sub>2</sub> in an outdoor chamber, dust chemistry at the low  
NO<sub>x</sub> level was attributed to 55% of total sulfate (56 ppb SO<sub>2</sub>, 290 µg m<sup>-3</sup> ATD, and NO<sub>x</sub> less than 5 ppb).  
At high NO<sub>x</sub> (>50 ppb of NO<sub>x</sub> with low hydrocarbons), sulfate formation was also greatly promoted by dust  
chemistry, but it was suppressed by the competition between NO<sub>2</sub> and SO<sub>2</sub> that both consume the dust-  
surface oxidants (OH radicals or ozone). The AMAR model, derived in this study with ATD particles, will  
30 provide a platform for predicting sulfate formation in the presence of authentic dust particles (e.g. Gobi and  
Saharan dust).

## 1 Introduction

The surface of mineral dust particles is able to act as a sink for various atmospheric trace gases such as sulfur dioxide ( $\text{SO}_2$ ), nitrogen oxides ( $\text{NO}_x$ , e.g.  $\text{NO}$  and  $\text{NO}_2$ ), and ozone ( $\text{O}_3$ ). Among trace gases,  $\text{SO}_2$  has received much attention because heterogeneous oxidation of  $\text{SO}_2$  produces nonvolatile sulfuric acid, which is readily involved in the acidification of particles or the reaction with dust constituents such as alkaline metals ( $\text{K}^+$ ,  $\text{Na}^+$ ) or metal oxides (e.g.  $\alpha\text{-Al}_2\text{O}_3$  and  $\text{Fe}_2\text{O}_3$ ). Such modification of the chemical composition of dust particles can influence the hygroscopic properties of mineral dust, which is essential to activate cloud condensation nucleation (Krueger et al., 2003; Zhang and Chan, 2002; Vlasenko et al., 2006; Liu et al., 2008; Tang et al., 2016).

Metal oxides (e.g.  $\text{TiO}_2$  and  $\text{Al}_2\text{O}_3$ ) have frequently been used in many laboratories to study the key role of mineral dust in the heterogeneous oxidation of  $\text{SO}_2$  (Goodman et al., 2001; Usher et al., 2002; Zhang et al., 2006). However, these laboratory studies have been limited to a certain type of metal oxide and autooxidation of  $\text{SO}_2$  without a light source. To date, only a few studies have attempted to study the photocatalytic characteristics of mineral dust in the oxidation of  $\text{SO}_2$  and  $\text{NO}_x$ . For example, as noted by Park and Jang (2016), the reactive uptake coefficient ( $\gamma_{\text{SO}_4^{2-}}$ ) of  $\text{SO}_2$  in the presence of dry Arizona Test Dust (ATD) particles under UV light was one order of magnitude higher ( $1.16 \times 10^{-6}$  using an indoor chamber with a light mix of UV-A and UV-B light) than that from autooxidation ( $1.15 \times 10^{-7}$ ) without a light source. Using an aerosol flow tube, Dupart et al. (2014) observed that the uptake rate of  $\text{NO}_2$  by ATD dust particles was significantly enhanced (by four times) under UV-A irradiation compared to dark conditions. Field observations have also reported the promotion of  $\text{SO}_2$  photooxidation in the presence of mineral dust. For instance, near Beijing, China (ground-based campaign in 2009), and in Lyon, France (remote-sensing campaign in 2010), Dupart et al. (2012) found that mineral dust was a source of OH radicals under UV radiation that promoted sulfate formation.

Semiconducting metal oxides (e.g.  $\alpha\text{-Al}_2\text{O}_3$ ,  $\alpha\text{-Fe}_2\text{O}_3$ , and  $\text{TiO}_2$ ) act as a photocatalyst in mineral dust particles that can yield electron ( $e^-_{\text{cb}}$ )–hole ( $h^+_{\text{vb}}$ ) pairs, and that they are involved in the production of strong oxidizers, such as superoxide radical anions ( $\text{O}_2^-$ ) and OH radicals (Linsebigler et al., 1995; Hoffmann et al., 1995; Thompson and Yates, 2006; Cwierz et al., 2008; Chen et al., 2012; Dupart et al., 2014; Colmenares and Luque, 2014). These oxidizers enable

rapid oxidation of adsorbed SO<sub>2</sub> and NO<sub>x</sub> on the surface of mineral dust particles. For example, using transmission FTIR spectroscopy and X-ray photoelectron spectroscopy, Nanayakkara et al. (2012) observed the oxidation of SO<sub>2</sub> by the photo-catalytically generated OH radicals in the presence of titanium oxide particles. The heterogeneous formation of sulfate and nitrate can be highly variable and dependent on the chemical characteristics of dust aerosol (Gankanda et al., 2016). Authentic mineral dust particles differ from pure metal oxides in chemical composition. For example, Wagner et al. (2012) reported that the content of metal oxides in Saharan dust samples from Burkina Faso includes 14% Al<sub>2</sub>O<sub>3</sub>, 8.4% Fe<sub>2</sub>O<sub>3</sub>, and 1.2% TiO<sub>2</sub>.

Most research on dust photochemistry has been limited to qualitative studies and lacks kinetic mechanisms that are linked to a predictive model. The typical wave-dependent photolysis of gas-phase trace gases has long been subject to atmospheric photochemistry. This photolysis rate is a first-order reaction and is calculated *via* the coupling actinic flux (the quantity of photons) with the characteristics (cross section area and quantum yield) of a light-absorbing molecule (McNaught and Wilkinson, 1997). In order to model dust photochemistry, the integration of wavelength-dependent actinic flux with the photocatalytic activity of mineral dust is needed.

In addition to sunlight intensity, humidity also influences heterogeneous dust chemistry. Humidity governs particle water content, which influences the gas-dust sorption process of trace gases (Navea et al., 2010) and the formation of dust-phase oxidants. Huang et al. (2015) found that the  $\gamma_{SO_4^{2-}}$  of SO<sub>2</sub> autooxidation in ATD particles increased by 142% because of the relative humidity (RH) changed from 15% to 90%. In the presence of UV light, the particle water content can act as an acceptor for  $h^+_{\nu b}$  and produce surface OH radicals, promoting heterogeneous photochemistry of SO<sub>2</sub> on mineral dust. In the presence of UV light, Shang et al. (2010) reported that sulfate production on the surface of TiO<sub>2</sub> increased by five times because of the increase of RH from 20% to 80%. Park and Jang (2016) also reported the exponential increase in  $\gamma_{SO_4^{2-}}$  as the RH increased from 20% to 80% for both autooxidation and photooxidation of SO<sub>2</sub> in the presence of ATD particles. A few studies have attempted to simulate sulfate formation in the presence of mineral dust at regional scales using laboratory-generated kinetic parameters (Tang et al., 2004; Li and Han, 2010; Dong et al., 2016). However,  $\gamma_{SO_4^{2-}}$  applied to the regional simulations originated from pure and dry metal oxides without UV light, and thus will differ from those of ambient dust exposed to natural sunlight. It is expected that the typical regional simulations during dust events might underestimate the formation of sulfate.



In this study, the Atmospheric Mineral Aerosol Reaction (AMAR) model was developed to predict atmospheric oxidation of trace gases such as SO<sub>2</sub> and NO<sub>2</sub> under ambient conditions. The kinetic mechanisms of dust-driven photochemistry, including autoxidation and photooxidation of SO<sub>2</sub>, was newly established in the model. The rate constant of dust photoactivation, which forms electron-hole pairs and sources dust-driven oxidants, was integrated into the model. The influence of meteorological variables, such as humidity, temperature and sunlight, on SO<sub>2</sub> oxidation was investigated using the resulting AMAR model. The model also addresses the kinetic mechanism to simulate how atmospheric major pollutants such as NO<sub>x</sub> and ozone are engaged in the oxidation of SO<sub>2</sub> in the presence of airborne dust particles. For environmental scenarios, the model was applied for polluted urban conditions (e.g. hydrocarbon ppbC/NO<sub>x</sub> ppb < 5) and low NO<sub>x</sub> conditions (e.g. hydrocarbon ppbC/NO<sub>x</sub> ppb > 5). The reaction rate constants for both autoxidation and photocatalytic reactions of SO<sub>2</sub> were obtained through the simulation of indoor chamber data, which were previously generated under various meteorological and environmental conditions (Park and Jang, 2016). The suitability of the resulting AMAR model was tested against sulfate formation in a large outdoor smog chamber at the University of Florida Atmospheric Photochemical Outdoor Reactor (UF-APHOR) under natural sunlight. The AMAR model of this study will vastly improve the accuracy of the prediction of sulfate and nitrate formation in regional and global scales where dust emission is influential.

## 2 Experimental section

### 2.1 Chamber experiments

The indoor chamber data of this study was obtained from the recent laboratory study by Park and Jang (2016) to determine the kinetic rate constants that are needed to develop the AMAR model. The indoor chamber operation has been reported previously (Park and Jang 2016) (Also see Sect. S1). The indoor chamber data are listed in Table 1. The outdoor chamber experiments were performed in the UF-APHOR dual chambers (52 m<sup>3</sup> for each chamber) to test the suitability of AMAR model to ambient condition. The light irradiation of the indoor-UV light and the sunlight are shown in Fig. S1. The detailed description of the operation of outdoor chamber is also described in Sect. S1. The outdoor experimental conditions for SO<sub>2</sub> heterogeneous reaction in the presence of mineral dust particles are listed in Table 2.

## 2.2 Light absorption of ATD particles

The absorbance spectrum of ATD particles was measured to develop the reaction rate constants in the kinetic model. The detailed procedure for light absorption measurement of particle samples can be found in the previous study (Zhong and Jang, 2011). The particle size distribution of ATD is shown in Fig. S2. The suspended dust particles were sampled on a Teflon coated glass fiber filter for 20 minutes. The masses difference of dust sample was measured using a microbalance (MX5, Mettler Toledo, Columbus, OH). The light absorbance of the dust filter sample ( $Ab_{S_{ATD}}$ ) was measured using a Perkin–Elmer Lambda 35 UV–visible spectrophotometer equipped with a Labsphere RSA–PE–20 diffuse–reflectance accessory. The absorbance spectrum was normalized by particle mass and calculated to obtain the mass absorbance cross section (See Sect. S1 in Supporting Information). The resulting absorbance cross section and quantum yield of ATD dust are shown in Fig. S3.

## 3 AMAR model description

The overall schematic of the AMAR model is shown in Fig 1. In the model, the total sulfate mass concentration ( $[SO_4^{2-}]_T$ ,  $\mu\text{g m}^{-3}$ ) is predicted from the reactions in three phases: the sulfate formed in the gas phase ( $[SO_4^{2-}]_{\text{gas}}$ ,  $\mu\text{g m}^{-3}$ ), the sulfate from the aqueous phase ( $[SO_4^{2-}]_{\text{aq}}$ ,  $\mu\text{g m}^{-3}$ ) and the sulfate from dust–driven chemistry ( $[SO_4^{2-}]_{\text{dust}}$ ,  $\mu\text{g m}^{-3}$ ). The key components of the model consist of the partitioning process and the kinetic mechanisms in three phases.

(1) The gaseous inorganic species (e.g.  $\text{SO}_2$ ,  $\text{NO}_x$  and ozone) are partitioned onto both inorganic–salt (sulfuric acid and its salts) seeded aqueous particles and mineral dust particles. The ~~gas–particle~~ partitioning processes between the gas phase and multilayer coated dust were treated by the ~~absorption~~adsorption–desorption kinetic mechanism.

(2)  $\text{SO}_2$  oxidation in the gas phase is simulated using mechanisms previously reported in the literature (Byun and Schere, 2006; Sarwar et al., 2013; Sarwar et al., 2014; Binkowski and Roselle, 2003) (Table. S1).

(3) The partitioned  $\text{SO}_2$  is heterogeneously oxidized in the inorganic–salt seeded aqueous phase based on the previously reported mechanisms (Liang and Jacobson, 1999).

(4) The formation of sulfate ( $[\text{SO}_4^{2-}]_{\text{dust}}$ ) in the dust phase is approached using two kinetic sub-modules: the production of sulfate ( $[\text{SO}_4^{2-}]_{\text{auto}}$ ,  $\mu\text{g m}^{-3}$ ) by autoxidation in open air and sulfate formation ( $[\text{SO}_4^{2-}]_{\text{photo}}$ ,  $\mu\text{g m}^{-3}$ ) by photocatalytic reactions.

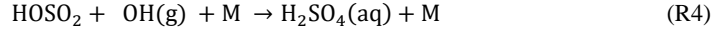
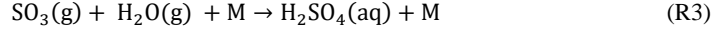
~~The rate constants associated with various reaction mechanisms in the AMAR model were determined by simulating indoor chamber data obtained from controlled experimental conditions (Table 1).~~ The simulation of chamber data using the model was performed using a kinetic solver (Morpho) (Jeffries, 1998). In these mechanisms, the symbols “g”, “aq”, and “d” denote the chemical species in the gas phase, inorganic-salt seeded aqueous phase, and dust phase, respectively. The unit of concentration of chemical species is molecule per  $\text{cm}^3$  of air. The rate constants associated with various reaction mechanisms in the AMAR model were determined by simulating pre-existing indoor chamber data obtained from controlled experimental conditions (Park and Jang, 2016). For example, the rate constant for  $\text{SO}_2$  autoxidation ( $k_{\text{auto}}$ ,  $\text{s}^{-1}$ ) is semiempirically determined by fitting the predicted concentration of sulfate to the experimental data D1 in Table 1. The gas-dust partitioning constant ( $K_{d, \text{SO}_2}$ , Sect. 3.2.1) of  $\text{SO}_2$  is dependent on temperature, aerosol water content, and acidity.  $K_{d, \text{SO}_2}$  values were semiempirically determined using data D1–D3 (three different RHs) and the literature parameters related to the effect of temperature and acidity on  $K_{d, \text{SO}_2}$ . The rate constant ( $k_{\text{photo}}$ ,  $\text{cm}^3 \text{ molecule}^{-1} \text{ s}^{-1}$ ) for the sulfate formation by photocatalytic reactions is semiempirically determined using data L1–L3 (three different RHs) in Table 1. In the presence of ozone,  $k_{\text{auto}}$  and  $k_{\text{photo}}$  are determined using datasets D4 and L4, respectively. In the following sections, the components of the AMAR model are described in detail.

### 3.1 $\text{SO}_2$ oxidation in gas phase and aerosol aqueous phase

#### 3.1.1 Gas phase oxidation

The oxidation of  $\text{SO}_2$  in the gas phase has been extensively studied by numerous researchers (Baulch et al., 1984; Kerr, 1984; Atkinson and Liody, 1984; Calvert, 1984; Graedel, 1977; Atkinson et al., 1997). In this study, the oxidation of  $\text{SO}_2$  is described using comprehensive reaction mechanisms shown in Table S1. The mechanisms can also be simplified as follows:



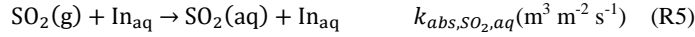


### 3.1.2 Gas–aerosol partitioning

SO<sub>2</sub> is dissolved into hygroscopic sulfuric acid (H<sub>2</sub>SO<sub>4</sub>), which is formed in the gas phase, via a partitioning process and reacts with the aqueous phase oxidants (e.g. H<sub>2</sub>O<sub>2</sub> and O<sub>3</sub>) to heterogeneously form H<sub>2</sub>SO<sub>4</sub>. The chemical species that were treated by the partitioning process include SO<sub>2</sub>, NO<sub>x</sub>, O<sub>3</sub>, OH, HO<sub>2</sub>, H<sub>2</sub>O<sub>2</sub>, HCOOH, CH<sub>3</sub>OOH, HNO<sub>3</sub>, CH<sub>3</sub>O<sub>2</sub>, HONO, CH<sub>3</sub>COOH, and HCHO. In the model, the partitioning process is approached using the gas–particle partitioning coefficient  $K_{aq,SO_2}$  (m<sup>3</sup> μg<sup>-1</sup>) based on aerosol mass concentration.  $K_{aq,SO_2}$  is derived from Henry's law constant of SO<sub>2</sub> ( $K_{H,SO_2}$  = 1.2 mol L<sup>-1</sup> atm<sup>-1</sup> at 298K) (Chameides, 1984),

$$K_{aq,SO_2} = \frac{K_{H,SO_2} RT}{\rho_{aq}} \quad (1)$$

where  $R$  is the ideal gas constant (J K<sup>-1</sup> mol<sup>-1</sup>) and  $\rho_{aq}$  (g cm<sup>-3</sup>) is the density of the particle, which is calculated using inorganic thermodynamic model (E–AIM II) (Clegg et al., 1998; Wexler and Clegg, 2002; Clegg and Wexler, 2011) based on humidity and inorganic composition. The ~~absorption–desorption~~ partitioning process of SO<sub>2</sub> on inorganic aerosol (In<sub>aq</sub>, m<sup>2</sup> m<sup>-3</sup>) is expressed as,



$k_{abs,SO_2,aq}$  (s<sup>-1</sup> m<sup>3</sup> m<sup>-2</sup>) and  $k_{des,SO_2,aq}$  (s<sup>-1</sup>) are the ~~absorption~~ uptake rate constant and the desorption rate constant, respectively, and are calculated as follows,

$$k_{abs,SO_2,aq} = f_{abs,aq} \frac{\omega_{SO_2} f_{aq,M2S}}{4} \quad (2)$$

$$k_{des,SO_2,aq} = \frac{k_{abs,SO_2,aq}}{K_{aq}} \quad (3)$$

where  $f_{aq,M2S}$  ( $5 \times 10^{-4}$ ) is the coefficient to convert the aerosol mass concentration (μg m<sup>-3</sup>) to the surface area concentration (m<sup>2</sup> m<sup>-3</sup>) for particle size near 100 nm and  $f_{abs,aq}$  is the coefficient for ~~absorption~~ uptake process.  $\omega_{SO_2}$  is the mean molecular velocity (m s<sup>-1</sup>) of SO<sub>2</sub> and can be calculated as follows,

$$\omega_{SO_2} = \sqrt{\frac{8RT}{\pi MW}} \quad (4)$$

where  $MW$  is molecular weight ( $\text{kg mol}^{-1}$ ). In our model,  $f_{abs,aq}$  was set at  $2 \times 10^4$  in Eq. (2) to have fast partitioning process. Table S2 summarizes the characteristic time that is estimated for diffusion, partitioning, and the reactions of major species with OH radicals in gas, aqueous, and dust phases. In general, the characteristic time (s) of a partitioning process (order of  $10^{-7}$  s) is much faster than gas phase oxidation (order of  $10^6$  s), aqueous phase oxidation (order of  $10^3$ – $10^4$  s), and dust phase oxidation (order of  $10^2$ – $10^3$  s at presence of  $200 \mu\text{g m}^{-3}$  of dust particles). The mass concentration ( $\mu\text{g m}^{-3}$ ) of inorganic seeded aqueous phase above the efflorescent relative humidity (ERH) is also dynamically calculated for the  $\text{SO}_4^{2-}$ – $\text{NH}_4^+$ – $\text{H}_2\text{O}$  system. Colberg et al. (2003) semiempirically predicted ERH by fitting to the experimental data based on the ammonia–to–sulfate ratio in the  $\text{SO}_4^{2-}$ – $\text{NH}_4^+$ – $\text{H}_2\text{O}$  system. AMAR model utilizes these parameterizations to predict ERH dynamically. Ammonia is inevitable in our chamber study and mainly acts as a carryover ~~for sulfate~~ from previous chamber experiments. Thus,  $\text{H}_2\text{SO}_4$  is fully or partially neutralized by ammonia.

### 3.1.3 Aerosol aqueous phase reaction

The AMAR model implements the aqueous–phase chemistry that occurs in inorganic salted aqueous aerosol ( $\text{SO}_4^{2-}$ – $\text{NH}_4^+$ – $\text{H}_2\text{O}$  system without dust) to form  $\text{SO}_4^{2-}(\text{aq})$  and  $\text{NO}_3^-(\text{aq})$ . We employed the preexisting aqueous–phase kinetic reactions involving  $\text{SO}_2$  (Liang and Jacobson, 1999) and  $\text{NO}_x$  chemistry (Liang and Jacobson, 1999; Hoyle et al., 2016). Thus, our simulation inherits all the possible uncertainties embedded in the original kinetic data.

The  $\text{SO}_2$  dissolved in the aqueous phase is hydrolyzed into  $\text{H}_2\text{SO}_3$  and dissociates to form ionic species ( $\text{HSO}_3^-$  and  $\text{SO}_3^{2-}$ ).  $\text{SO}_4^{2-}(\text{aq})$  is formed by reactions of the sulfur species in oxidation state IV ( $\text{S(IV)}(\text{aq})$ ) with  $\text{OH}(\text{aq})$ ,  $\text{H}_2\text{O}_2(\text{aq})$ , or  $\text{O}_3(\text{aq})$  (Table S1). The dissolved HONO can also dissociate to form  $\text{NO}_2^-(\text{aq})$  and result to  $\text{NO}_3^-(\text{aq})$ . Each chemical species in  $\text{S(IV)}(\text{aq})$  has a different reactivity for oxidation reactions. The distribution of chemical species is affected by aerosol acidity, which is controlled by humidity and inorganic composition. Hence, the formation of sulfate is very sensitive to aerosol acidity. For example, most of the  $\text{S(IV)}$  is consumed by  $\text{H}_2\text{O}_2$  at  $\text{pH} < 4$ , whereas most of it is consumed by  $\text{O}_3$  at  $\text{pH} > 4$ . Some strong inorganic acids, such as sulfuric acid, influence aerosol acidity. In AMAR, aerosol acidity ( $[\text{H}^+]$ ,  $\text{mol L}^{-1}$ ) is ~~predicted using the inorganic thermodynamic model~~ estimated at each time step by E-AIM II (Clegg et al., 1998; Wexler and Clegg, 2002; Clegg and Wexler, 2011) ~~based on the ammonia–to–sulfate ratio~~

~~and RH-corrected for the ammonia rich condition (Li et al., 2015; Beardsley and Jang, 2016; Li and Jang, 2012) as a function of inorganic composition measured by a Particle Into-Liquid Sampler coupled with Ion Chromatography (PILS-IC).~~ When the ammonia-to-sulfate ratio is greater than 0.8, the prediction of  $[H^+]$  is corrected based on the method of Li and Jang (2012). At high  $NO_x$  levels,  $NO_2^-(aq)$  competes with  $S(IV)(aq)$  for the reaction with  $OH(aq)$ ,  $O_3$ , or  $H_2O_2$  (Table S1)(Ma et al., 2008). However, the HONO concentration becomes high at high  $NO_x$  levels and enhances  $SO_2$  oxidation in the inorganic-salt seeded aqueous phase due to the formation of OH radicals *via* photolysis of HONO.

### 3.2 Heterogeneous oxidation in the presence of mineral dust particles

The heterogeneous chemistry in the presence of dust particles has been newly established in the AMAR model. The dust phase module consists of a partitioning process (Sect. 3.2.1) and heterogeneous chemistry for  $SO_2$  and other trace gases (ozone, HONO, and  $NO_2$ ) (Table 3) (Fig. 1). The heterogeneous chemistry of  $SO_2$  is handled by autooxidation (Sect. 3.2.2) and photooxidation under UV light (Sect. 3.2.4). In dust-phase photochemistry, the central mechanism for  $SO_2$  oxidation is operated by the surface oxidants (e.g.  $OH(d)$ ), which is generated *via* the photoactivation process of semiconductive metal oxides in dust particles (Sect. 3.2.3).

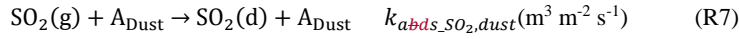
#### 3.2.1 Gas-dust particle partitioning

In an adsorptive mode, water molecules suppress partitioning of  $SO_2$  because they compete for adsorptive sites with tracers (Cwiertny et al., 2008). However, the formation of the sulfate associated with ATD increased as increasing RH as shown in Table 1, suggesting that gas-dust partitioning is more likely operated by ~~an absorption process~~ adsorption on the multilayer coated dust with water molecules. ATD contains hygroscopic inorganic salts that form the thin water film on the surface of ATD particles when the salts are deliquescent (or above ERH). This water layer influences the gas-dust partitioning of atmospheric tracers such as  $SO_2$  and  $NO_2$ . The gas-dust partitioning constant ( $K_{d,SO_2}$ ,  $m^3 m^{-2}$ ) of  $SO_2$  is defined as,

$$K_{d,SO_2} = \frac{[SO_2]_d}{[SO_2]_g A_{Dust}} \quad (m^3 m^{-2}) \quad (5)$$

$A_{dust}$  ( $m^2 m^{-3}$ ) is the geometric surface concentration of ATD dust particles and is calculated by multiplying the dust mass concentration ( $\mu g m^{-3}$ ) by a geometric surface-mass ratio ( $f_{dust,M2S}$ ) of

ATD particles ( $3.066 \times 10^{-6}$ ,  $\text{m}^2 \mu\text{g}^{-1}$ ). The  $\text{SO}_2$  ~~absorption~~adsorption and desorption processes for the dust phase are expressed as



5  $k_{\text{ads}_{\text{SO}_2, \text{dust}}} (\text{s}^{-1} \text{m}^3 \text{m}^{-2})$  and  $k_{\text{des}_{\text{SO}_2, \text{dust}}} (\text{s}^{-1})$  are the ~~absorption~~adsorption rate constant and the desorption rate constant, respectively. At equilibrium, the ~~absorption~~adsorption rate (R7) equals the desorption rate (R8). Thus,  $K_{\text{d}, \text{SO}_2}$  can be expressed as

$$K_{\text{d}, \text{SO}_2} = \frac{k_{\text{ads}_{\text{SO}_2, \text{dust}}}}{k_{\text{des}_{\text{SO}_2, \text{dust}}}} (\text{m}^3 \text{m}^{-2}) \quad (6)$$

The  $K_{\text{d}, \text{SO}_2}$  value at 20% RH is set at  $1.63 (\text{m}^3 \text{m}^{-2}, \text{at } 298\text{K for dry particles})$  based on the literature data (dust particles at 20% RH) (Adams et al., 2005; Huang et al., 2015). The characteristic time to reach to equilibrium is very short (Sect. 3.1.1). In kinetic mechanisms,  $k_{\text{ads}_{\text{SO}_2, \text{dust}}}$  was set at  $1.7 \times 10^3 \text{ s}^{-1} \text{m}^3 \text{m}^{-2}$  for dry particles (20% RH) using the same approach as Eq. (2). The resulting characteristic time for  $k_{\text{ads}_{\text{SO}_2, \text{dust}}}$  is  $10^{-6} \text{ s}$ . The characteristic time of the reaction of  $\text{SO}_2$  with an OH radical ( $10^6 \text{ molecules cm}^{-3}$ ) is about  $10^6$ – $10^7 \text{ s}$  in gas phase and  $10^5$ – $10^6 \text{ s}$  in both aqueous  
15 phase and dust phase.

To consider the effect of temperature on  $K_{\text{d}, \text{SO}_2}$ , the temperature dependency of  $k_{\text{des}_{\text{SO}_2, \text{dust}}}$  (Eq. (6)) is derived from the Henry's constant (Chameides, 1984).  $K_{\text{d}, \text{SO}_2}$  (Eq. (5)) is also influenced by aerosol water content (Zuend et al., 2011) as well as the dissociation of  $\text{H}_2\text{SO}_3$ , which is operated by aerosol acidity ( $[\text{H}^+]$ ) and an acid dissociation constant ( $K_{\text{aSO}_2}$ ) (Martell and  
20 Smith, 1976). Thus,  $k_{\text{des}_{\text{SO}_2, \text{dust}}}$  is expressed as,

$$k_{\text{des}_{\text{SO}_2, \text{dust}}} = 1 \times 10^9 \exp\left(-\frac{3100}{T}\right) / (F_{\text{water}}(1 + \frac{K_{\text{aSO}_2}}{[\text{H}^+]}) (\text{s}^{-1}) \quad (7)$$

$K_{\text{aSO}_2}$  is  $0.013 (\text{mol L}^{-1})$  at 298K (Martell and Smith, 1976). The influence of the dissociation of inorganic acid on  $K_{\text{d}, \text{SO}_2}$  is accounted for by the term  $(1 + \frac{K_{\text{aSO}_2}}{[\text{H}^+]})$  in Eq. (7). The estimation of  $[\text{H}^+]$  is treated in the same ways as aqueous chemistry (Sect. 3.1.3).

25 In order to estimate  $K_{\text{d}, \text{SO}_2}$  at different RH,  $F_{\text{water}}$ , a numeric number, (coefficient of the mass fraction of water to dust particles) was introduced into the model ~~to estimate the water fraction of total dust particles.~~ The hygroscopic property of mineral dust dynamically changes because dust can be substantially modified by direct reaction of some of its components (e.g.

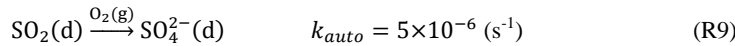
CaCO<sub>3</sub>) with inorganic acids such as H<sub>2</sub>SO<sub>4</sub> and HNO<sub>3</sub>. When dust forms Ca(NO<sub>3</sub>)<sub>2</sub>, dust becomes more hygroscopic. Nitrate salts deliquesce at very low RH (17%) (Krueger et al., 2003; Krueger et al., 2004; William et al., 2005). CaSO<sub>4</sub> is, however, relatively hydrophobic. Nitrate salts exist only when sulfate concentrations is very low. In the model,  $F_{water}$  originated from is associated with  
 5 the hygroscopic property of indigenous dust (first term in Eq. (8)), the inorganic nitrates formed from the reaction of ~~absorbed~~adsorbed HNO<sub>3</sub> with dust (second term), and the inorganic sulfate (SO<sub>4</sub><sup>2-</sup>-NH<sub>4</sub><sup>+</sup>-H<sub>2</sub>O system, third term).

$$F_{water} = \exp(4.4RH) + 3.7\exp(4.4RH) \frac{[NO_3^-(d\_salt)]}{[Dust]} + \frac{M_{in,water}}{[Dust]} \quad (8)$$

$M_{in,water}$  is the water concentration ( $\mu\text{g m}^{-3}$ ) associated with inorganic sulfate and calculated using  
 10 E-AIM II. Both  $[NO_3^-(d\_salt)]$  and  $M_{in,water}$  are normalized by the mass concentration of ATD particles ( $[Dust]$ ,  $\mu\text{g cm}^{-3}$ ).  $F_{water}$  is first determined using chamber simulation of SO<sub>2</sub> heterogeneous oxidation (first and third terms in Eq. (8)) (D1-D3 in Table 1) under varied RH levels and extended to SO<sub>2</sub> oxidation in the presence of NO<sub>x</sub> (Exp. 14 April 2017 in Table 2). Among temperature, RH and aerosol acidity, the most influential variable is RH due to the  
 15 variation of  $F_{water}$  (see sensitivity analysis in Sect. 5).

### 3.2.2 Autoxidation of SO<sub>2</sub> on dust surface

Typically, autoxidation of SO<sub>2</sub> is an oxidation process *via* the reaction of ~~absorbed~~adsorbed SO<sub>2</sub> (R7 and R8) with an oxygen molecule. In the model,  $[SO_4^{2-}]_{auto}$  is defined as the sulfate resulted from any oxidation reactions (autoxidation in open air and oxidation with ozone) of SO<sub>2</sub>  
 20 without UV light (Fig. 1). In autoxidation, the reaction of SO<sub>2</sub>(d) with the oxygen molecules is treated as the first order reaction (assuming the concentration of oxygen is constant as  $2 \times 10^5$  ppm).



In the dark condition, the formation of sulfate is mainly sourced from autoxidation of SO<sub>2</sub>. ~~By fitting the predicted concentration of sulfate to the experimental data (D1-D3 in Table 1), the reaction rate constant ( $k_{auto}$ , s<sup>-1</sup>) for SO<sub>2</sub> autoxidation is semiempirically determined.~~ For  
 25 comparison with other studies, we estimate the reactive uptake coefficient ( $\gamma_{SO_4^{2-},auto}$ ) of SO<sub>2</sub> onto ATD dust in the absence of ozone and NO<sub>x</sub> (Fig. 2).

$$\gamma_{SO_4^{2-},auto} = \frac{4K_{d,SO_2}k_{auto}}{\omega_{SO_2}} \quad (9)$$

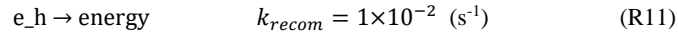
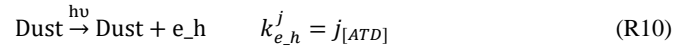


$\gamma_{SO_4^{2-}, auto}$  is proportional to  $K_{d, SO_2}$ , and influenced by humidity (Eq. (7)).

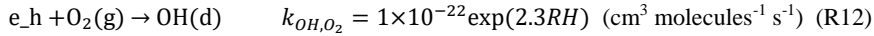
### 3.2.3 Photoactivation of dust particles and heterogeneous formation of OH radicals

The reactive uptake of  $SO_2$  on particles is traditionally treated as a first order process (Ullerstam et al., 2003; Li et al., 2007). Such an approach is appropriate for simple autoxidation mechanisms, but not for the complex heterogeneous photooxidation of  $SO_2$ . In the AMAR model, the heterogeneous photooxidation of  $SO_2$  is approached in three steps: (1) the formation of an  $e^-_{cb}-h^+_{vb}$  pair *via* photoactivation of dust particles, (2) the formation of OH(d) *via* the reaction of an  $e^-_{cb}-h^+_{vb}$  pair with a water or oxygen molecule, and (3) the reaction of ~~absorbed~~adsorbed  $SO_2$  with the resulting OH(d) (second-order reactions) (Table S1).

The photoactivation of dust particles and the recombination reaction of an electron-hole pair ( $e^-_h$ ) are added into the model.



where  $k_{e^-_h}^j$  is the photoactivation rate constant to form  $e^-_{cb}-h^+_{vb}$  pairs and  $k_{recom}$  is the reaction rate constant of recombination (heat radiation) of an electron and a hole. The value of  $k_{recom}$  is set at a large number to prevent the accumulation of electron-hole pairs. The formation of OH(d) is expressed as



$k_{OH, O_2}$  is the reaction rate constant to form OH(d) and is first estimated using indoor chamber data

(L1–L3 in Table 1) at RH 20%, 55% and 80% and then regressed against RH. The study by Thiebaud et al. (2010) reported the recombination of OH(d) near to  $TiO_2$  surfaces. In our model, the mechanistic role of the catalytic formation of the electron-hole pairs (R10) and their recombination (R11) compensates the formation and the self-reaction of OH radicals.

In R10,  $k_{e^-_h}^j$  is the operational rate constant for the photoactivation of dust particles and is dependent on the photolysis rate constant,  $j_{[ATD]}$  ( $s^{-1}$ ). Like the typical photolysis of a gaseous molecule, the photocatalytic production of  $e^-_{cb}-h^+_{vb}$  pairs is linear to both the actinic flux ( $I(\lambda)$ , photons  $cm^{-2} nm^{-1} s^{-1}$ ) originating from the light source and the photocatalytic property of dust particles. The value of  $j_{[ATD]}$  is determined by  $I(\lambda)$ , the absorption cross section ( $\sigma(\lambda)$ ,  $cm^2 \mu g^{-1}$ ), and the quantum yield ( $\phi(\lambda)$ ) of dust conducting matter at each wavelength range ( $\lambda$ , nm),

$$j_{[ATD]} = \int_{\lambda_1}^{\lambda_2} I(\lambda) \sigma(\lambda) \phi(\lambda) d\lambda \quad (10)$$

In the model,  $\sigma(\lambda)$  is the light absorption needed to activate dust-phase semiconducting metal oxides (excitation from a ground energy level to a conducting band), and  $\phi(\lambda)$  is the probability of yielding the  $e^-_{cb}-h^+_{vb}$  pair in the dust phase. Both  $\sigma(\lambda)$  and  $\phi(\lambda)$  cannot be directly measured because of complexity in the quantity of photoactive conducting matter in dust particles and the irradiation processes of the  $e^-_{cb}-h^+_{vb}$  pair. In order to deal with  $\sigma(\lambda) \times \phi(\lambda)$ , we calculated the mass absorption cross section of dust particles ( $MAC_{ATD}$ ,  $m^2 g^{-1}$ ), which was determined using the absorption coefficient of ATD particles ( $b_{ATD}$ ,  $m^{-1}$ ) with the particle concentration ( $m_{ATD}$ ,  $g m^{-3}$ ):

$$MAC_{ATD} = \frac{b_{ATD}}{m_{ATD}} \quad (11)$$

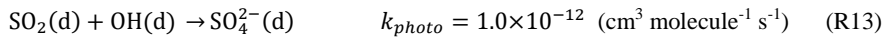
In Eq. (11),  $b_{ATD}$  can be calculated from the absorbance of dust filter sample ( $Abs_{ATD}$ , dimensionless) measured using a reflective UV–visible spectrometer (Fig. S3):

$$b_{ATD} = \frac{Abs_{ATD} A}{f V} \ln(10) \quad (12)$$

where  $A = 7.85 \times 10^{-5} (m^2)$  is the sampled area on the filter and  $V (m^3)$  is the total air volume passing through the filter during sampling. In order to eliminate the absorbance caused by filter material scattering, a correction factor ( $f = 1.4845$ ) is obtained from a previous study (Zhong and Jang, 2011) and coupled into Eq. (12). The preliminary study showed that the effect of aerosol scattering on the  $b_{abs}$  values of the aerosol collected on the filter was negligible. Further, Bond (2001) reported that particle light scattering does not significantly influence spectral absorption selectivity. The  $MAC_{ATD}$  of dust particles originates from photocatalytic conducting matter (e.g.  $TiO_2$ ) as well as light-absorbing matter (e.g. gypsum and metal sulfate). Thus, the  $MAC_{ATD}$  spectrum is adjusted using the known  $TiO_2$  absorption spectrum (Reyes–Coronado et al., 2008) and applied to  $\sigma(\lambda) \times \phi(\lambda)$  (Fig. S3). The resulting  $\sigma(\lambda) \times \phi(\lambda)$  spectrum is applied to Eq. (10) to calculate  $j_{[ATD]}$  (R10).

### 3.2.4 Heterogeneous photooxidation of $SO_2$

$SO_2$  is oxidized by  $OH(d)$  on the surface of ATD particles as follows,



where  $k_{photo}$  is the reaction rate constant of SO<sub>2</sub> with OH(d) and is estimated from gas phase reaction (R1). Combining Eq. (4), Eq. (5), R11 and R15, the reactive uptake coefficient ( $\gamma_{SO_4^{2-},photo}$ ) of SO<sub>2</sub> on ATD particles under UV light can be written as,

$$\gamma_{SO_4^{2-},photo} = \frac{4K_{d,SO_2}(k_{photo}[OH(d)] + k_{auto})}{\omega_{SO_2}} \quad (13)$$

5  $\gamma_{SO_4^{2-},photo}$  is the constant at a given concentration of OH(d) (for a given light source, dust concentration, and humidity) (R10 and R12). Figure 2 illustrates  $\gamma_{SO_4^{2-},photo}$  values at three different RHs, which were obtained using indoor chamber data.  $\gamma_{SO_4^{2-},photo}$  is significantly influenced by both UV light and humidity. For example,  $\gamma_{SO_4^{2-},photo}$  is one order of magnitude higher than  $\gamma_{SO_4^{2-},auto}$  at low NO<sub>x</sub> levels (<5 ppb), and  $\gamma_{SO_4^{2-},photo}$  increased from  $2.0 \times 10^{-5}$  to  
10  $1.24 \times 10^{-4}$  when the RH changed from 20% to 80%.

### 3.3 Impact of ozone and NO<sub>x</sub> on heterogeneous chemistry of SO<sub>2</sub>

To date, most studies of the effect of NO<sub>x</sub> on sulfate formation have been limited to the reaction in dark condition. For example, previous laboratory studies using pure metal oxides reported the acceleration of the heterogeneous oxidation of SO<sub>2</sub> by NO<sub>x</sub> in dark conditions (Ma et al., 2008; Liu et al., 2012). For the effect of ozone, the recent chamber study by Park and Jang (2016) showed significant enhancement of heterogeneous photooxidation of SO<sub>2</sub>. In the AMAR model, the formation of sulfate is also modulated by the involvement of ozone and NO<sub>x</sub> in both autoxidation and photochemistry on the surface of dust particles (Fig. 1).  
15

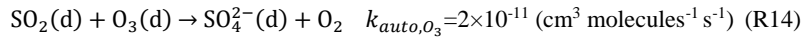
#### 3.3.1 Dust-phase ozone chemistry

20 The gas–dust partitioning coefficient of ozone is scaled using  $K_{d,SO_2}$  and the ratio of the Henry's law constant of SO<sub>2</sub> ( $K_{H,SO_2}$ , Eq. (1)) to that of ozone ( $K_{H,O_3} = 1.2 \times 10^{-2} \text{ mol L}^{-1} \text{ atm}^{-1}$  at 298K) (Chameides, 1984),

$$K_{d,O_3} = K_{d,SO_2} \frac{K_{H,O_3}}{K_{H,SO_2}} = 7.7 \times 10^{-7} F_{water} \exp\left(\frac{2700}{T}\right) \quad (\text{m}^3 \text{ m}^{-2}) \quad (14)$$

The partitioning process is also treated by the adsorption–desorption kinetic mechanism as shown  
25 in R7 and R8 (Table 3: partitioning). Ozone can decay catalytically in the dust phase, forming an oxygen molecule and surface-bound atomic oxygen (Usher et al., 2003; Chang et al., 2005). The

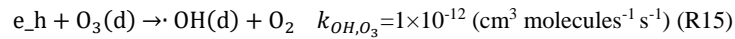
formed atomic oxygen reacts with SO<sub>2</sub>(d) to form sulfate (Ullerstam et al., 2002; Usher et al., 2002):



~~$k_{\text{auto},\text{O}_3}$  is estimated using indoor chamber data (D4 in Table 1).~~ In the presence of 300 µg m<sup>3</sup> of

5 ATD particles and 60 ppb of ozone, the concentration of O<sub>3</sub>(d) is estimated as  $2.4 \times 10^7$  molecule cm<sup>-3</sup>. Under this condition, the characteristic time of the autoxidation by ozone (R14) is  $2 \times 10^3$  s and is much faster than the autoxidation by oxygen (R9,  $2 \times 10^5$  s). At nighttime, in the presence of ozone, the autoxidation of SO<sub>2</sub>(d) yields a significant amount of sulfate.

10 Under UV light, ozone is also involved in the production of the surface oxidants (O<sub>3</sub><sup>·</sup>, HO<sub>3</sub> radicals, and OH radicals) that further promote heterogeneous oxidation of SO<sub>2</sub>. O<sub>3</sub>(d) acts as an acceptor for e<sup>-</sup><sub>cb</sub>-h<sup>+</sup><sub>vb</sub> and forms OH(d):



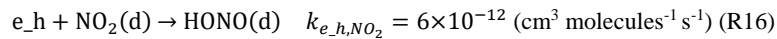
### 3.3.2 Dust-phase NO<sub>x</sub> chemistry

The gas-dust partitioning coefficient of NO<sub>2</sub> ( $K_{d,\text{NO}_2}$ ) is treated as the same approach 15 with ozone, using  $K_{d,\text{SO}_2}$  and the ratio of  $K_{H,\text{SO}_2}$  (Eq. (1)) to the Henry's law constant of NO<sub>2</sub> ( $K_{H,\text{NO}_2} = 1.2 \times 10^{-2} \text{ mol L}^{-1} \text{ atm}^{-1}$  at 298K) (Chameides, 1984):

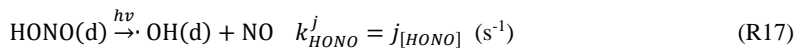
$$K_{d,\text{NO}_2} = K_{d,\text{SO}_2} \frac{K_{H,\text{NO}_2}}{K_{H,\text{SO}_2}} = 1.5 \times 10^{-6} F_{\text{water}} \exp\left(\frac{2500}{T}\right) \text{ (m}^3 \text{ m}^{-2}) \text{ (15)}$$

The ~~absorbed~~adsorbed NO<sub>2</sub> first reacts with e<sup>-</sup><sub>cb</sub>(d) or ·O<sub>2</sub><sup>-</sup>(d) on the dust surface (R10) and forms HONO(d) (Ma et al., 2008; Liu et al., 2012; Saliba and Chamseddine, 2012; Saliba et al., 2014).

20 In AMAR, the formation of HONO(d) is simplified into:

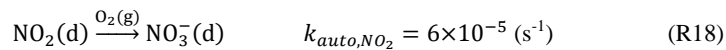


HONO(d) is further decomposed through photolysis and yields OH(d):

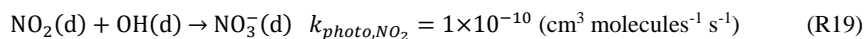


The photolysis rate constant of HONO(d) is treated with the one for gaseous HONO ( $j_{[\text{HONO}]}$ ).

25 Similar to autoxidation of SO<sub>2</sub> (Sect. 3.2.2), NO<sub>2</sub>(d) autoxidizes to form nitrate:



NO<sub>2</sub> reacts with OH(d):



$k_{auto,NO_2}$  and  $k_{photo,NO_2}$  was determined using the simulation of outdoor chamber data (Exp. 14 April 2017 in Table 2). The estimation of the gas–dust partitioning coefficients of HONO ( $K_{d,HONO}$ ) (Becker et al., 1996) and  $HNO_3$  ( $K_{d,HNO_3}$ ) (Schwartz and White, 1981) was approached using the similar method for  $SO_2$  (Table 3).  $N_2O_5$  forms nitrate *via* a reactive uptake process as shown in Table 3 (reaction 11).

#### 4 Simulation of AMAR model under ambient sunlight

At the beginning of the development of the AMAR model, the kinetic parameters to predict the formation of sulfate and nitrate in the presence of ATD particles were leveraged using an indoor chamber. In order to test the feasibility of the resulting AMAR model, the UF–APHOR data using natural sunlight were simulated (Table 2). The chamber dilution (measured by  $CCl_4$ ) and the wall process of gaseous compounds (e.g. ozone,  $SO_2$ , HONO,  $NO_2$ ) and particles were integrated with the kinetic mechanisms to simulate UF–APHOR data (Sect. S1). As shown in Fig. 1, the model inputs are the concentration of chemical species, the amount of dust, and the meteorological variables that are commonly found at regional scales. The dual chambers allow for two controlled experiments to be performed simultaneously under the same meteorological conditions.

##### 4.1 Simulations for different dust loadings

Figure 3 shows that the predicted  $[SO_4^{2-}]_T$  is in good agreement with experimental observations, which were performed under low  $NO_x$  conditions ( $NO_x < 5$  ppb) for two different dust loadings as well as two different  $SO_2$  levels. The greater increase in  $[SO_4^{2-}]_T$  appeared with the higher sunlight intensity (between 11 AM and 2 PM). In Fig. 3(a), the predicted  $[SO_4^{2-}]_T$  increased by 63% (at 3 PM) with  $290 \mu g m^{-3}$  of ATD particles compared to the  $[SO_4^{2-}]_T$  without dust particles. Figure 3(b) confirms that the larger dust particle loading yields more  $[SO_4^{2-}]_T$ . In Fig. 3(c),  $[SO_4^{2-}]_T$  was predicted with high and low initial concentrations of  $SO_2$  for a given dust loading. The time profiles of the simulation of concentrations of  $NO_x$ , ozone,  $SO_2$ , and dust are shown in Fig. S4.

Because of the large size of dust particles, the wall processes (e.g. settling and wall deposition) of dust particles is greater than that of the sulfate particles originated from  $[SO_4^{2-}]_{aq}$  (no dust). Hence, the fraction of  $[SO_4^{2-}]_{dust}$  to  $[SO_4^{2-}]_T$  declines over the course of the chamber experiment. To estimate how the predicted  $[SO_4^{2-}]_T$  is attributed to  $[SO_4^{2-}]_{aq} + [SO_4^{2-}]_{gas}$  (non–dust

sulfate) and  $[\text{SO}_4^{2-}]_{\text{dust}}$  without wall processes, Fig. 3(d), 3(e), and 3(f) are reconstructed from Fig. 3(a), 3(b), and 3(c), respectively. As shown in the inner pie chart of Fig. 3(d), a significant fraction of  $[\text{SO}_4^{2-}]_{\text{T}}$  is attributed to dust phase chemistry ( $[\text{SO}_4^{2-}]_{\text{auto}} + [\text{SO}_4^{2-}]_{\text{photo}} : 0.58$ ). In Fig. 3(e), the fraction of final  $[\text{SO}_4^{2-}]_{\text{photo}}$  to  $[\text{SO}_4^{2-}]_{\text{T}}$  increases from 0.28 to 0.72 with the increase of dust loading from  $90 \mu\text{g m}^{-3}$  to  $403 \mu\text{g m}^{-3}$ . The increased dust loading promotes both the ~~absorption~~adsorption of  $\text{SO}_2$  onto dust particles and the production of dust-phase oxidants, and thus yields more sulfate production. With the increase of the initial concentration of  $\text{SO}_2$  from 119 ppb to 272 ppb in Fig. 3(f), the fraction of  $[\text{SO}_4^{2-}]_{\text{photo}}$  and  $[\text{SO}_4^{2-}]_{\text{gas}} + [\text{SO}_4^{2-}]_{\text{aq}}$  are not much changed, while  $[\text{SO}_4^{2-}]_{\text{T}}$  increases from  $16.6 \mu\text{g m}^{-3}$  to  $30.1 \mu\text{g m}^{-3}$ . The elevation of the concentration of  $\text{SO}_2$  produces more sulfate in all three phases (gas, aqueous, and dust phases). The sulfuric acid formed in the aqueous phase is hydrophilic and creates a positive feedback loop which aggravates the growth of aqueous aerosol. Overall, the variation in dust concentration is more influential on  $[\text{SO}_4^{2-}]_{\text{photo}}$  than that of  $\text{SO}_2$ .

#### 4.2 Simulation of $\text{NO}_x$ effect

Figure 4 shows that the model performs well in predicting  $[\text{SO}_4^{2-}]_{\text{T}}$  in various levels of  $\text{NO}_x$ . Figure 4(d) is reconstructed from Fig. 4(a), 4(b) and 4(c) to illustrate how  $[\text{SO}_4^{2-}]_{\text{T}}$  is attributed to the aqueous-phase reaction ( $[\text{SO}_4^{2-}]_{\text{gas}} + [\text{SO}_4^{2-}]_{\text{aq}}$ ), dust-phase autoxidation ( $[\text{SO}_4^{2-}]_{\text{auto}}$ ), and dust photochemistry ( $[\text{SO}_4^{2-}]_{\text{photo}}$ ). Comparing Fig. 4(b) with 4(c),  $[\text{SO}_4^{2-}]_{\text{photo}}$  is suppressed at high  $\text{NO}_x$  levels because  $\text{NO}_2$  competes for the consumption of dust-phase OH radicals with  $\text{SO}_2$ . The reduction of  $[\text{SO}_4^{2-}]_{\text{T}}$  in the afternoon is due to the particle loss at the low concentrations of  $\text{SO}_2$ . The simulated concentrations of  $\text{NO}_x$ , ozone,  $\text{SO}_2$ , and dust are shown in Fig. S5.

The time profiles of the predicted  $[\text{NO}_3^-]_{\text{T}}$  are also shown in Fig. 4(a), 4(b), and 4(c). In the morning,  $\text{NO}_2$  quickly oxidizes to accumulate nitric acid in the dust phase. The dust-phase nitric acid might rapidly react with alkaline carbonates (e.g. K, Na, Ca and Mg ions) in the dust phase and form nitrate salts ( $\text{NO}_3^- (\text{d\_salt})$ ) in reaction 23 of dust phase reactions in Table S1). As described in Sect. 3.2.1, these nitrate salts are very hygroscopic and further enhance gas-dust partitioning of gaseous species including  $\text{HNO}_3$ ,  $\text{SO}_2$ , and  $\text{HONO}$  at high humidity (in the morning). With increasing sunlight intensity, the temperature increases but humidity decreases (20%, Fig. S6) and thus increase the desorption of  $\text{HNO}_3$ . In addition to meteorological conditions,

the formation of low-volatility sulfuric acid can deplete nitrate *via* evaporation of volatile nitric acid ( $\text{SO}_4^{2-}$  (d\_salt) in reaction 24 and 25 of dust phase reactions in Table S1) from the dust surface. The capacity of ATD particles to form nitrate salts (or sulfate salts) is limited by the amount of carbonates and metal oxides on the surface of dust particles. This capacity is estimated to be 0.6 ppb (the number concentration of reactive sites in air), which was determined by comparing the actual aerosol acidity, as measured by the colorimetry integrated with a reflectance UV-visible spectrometer (C-RUV), to the aerosol acidity predicted by the inorganic thermodynamic model (E-AIM II) using the inorganic composition from PILS-IC (Li et al., 2015; Beardsley and Jang, 2016). As shown in Fig. 4, the effect of  $\text{HNO}_3$  on the heterogeneous reaction is negligible during the daytime because sulfuric acid, a strong acid, depletes partitioning of  $\text{HNO}_3$  (Eq. (15)). At the end of the photooxidation, nitrate is slightly underestimated because some observed nitrate may be trapped under the layer of hydrophobic alkaline sulfate formed *via* aging of ATD particles (effloresced). The surface  $\text{HONO(d)}$ , which formed *via* the photocatalytic process of  $\text{NO}_2$  (R16), can influence the production of  $\text{OH(d)}$ . However, the model analysis originated from the integrated reaction rate (IRR), an accumulated flux of chemical formation, suggests that the contribution of  $\text{HONO(d)}$  to  $\text{OH(d)}$  production is relatively small compared to the direct photocatalytic process caused by dust particles shown in Sect. 3.2.3.

## 5 Sensitivity and uncertainties

The sensitivity of sulfate prediction to major variables (e.g. temperature, humidity, sunlight profile, the concentration of  $\text{SO}_2$  and  $\text{NO}_x$ , and dust loading) is illustrated in Fig. 5. To avoid the suppression of dust chemistry at high  $\text{NO}_x$  levels, the most sensitivity tests were performed at low levels of  $\text{NO}_x$ . The stacked chart normalized with  $[\text{SO}_4^{2-}]$  in Fig. 5 shows how  $[\text{SO}_4^{2-}]_{\text{T}}$  is attributed to  $[\text{SO}_4^{2-}]_{\text{auto}}$ ,  $[\text{SO}_4^{2-}]_{\text{photo}}$  and  $[\text{SO}_4^{2-}]_{\text{aq}} + [\text{SO}_4^{2-}]_{\text{gas}}$  (non-dust chemistry).

Figure 5(a) illustrates that the reduction of  $[\text{SO}_4^{2-}]_{\text{T}}$  at a higher temperature (273K vs. 298K) is ascribed to the decrease in the partitioning process. Figure 5(b) shows that  $[\text{SO}_4^{2-}]_{\text{T}}$  increases by a factor of 2.8 with RH increasing from 25% to 80%. Humidity plays an important role in the modulation of both aerosol acidity and liquid water content, and ultimately influences the partitioning process (e.g.  $\text{SO}_2$  partitioning on dust surface) and dust-phase chemistry (e.g. production of  $\text{OH(d)}$ ). In the stacked column chart of Fig. 5(b), the contribution of  $[\text{SO}_4^{2-}]_{\text{dust}}$  to  $[\text{SO}_4^{2-}]_{\text{T}}$  increases from 0.73 to 0.86 with increasing RH suggesting that dust chemistry is more

sensitive to humidity than aqueous phase chemistry. Figure 5(c) presents  $[\text{SO}_4^{2-}]_T$  at two different sunlight intensities (winter on 12 November, 2015 vs. summer on 25 April, 2017) in Gainesville, Florida (latitude/longitude: 29.64185°/-82.347883°). As shown in Fig. 5(d), with  $\text{SO}_2$  concentrations increasing from 20 ppb to 100 ppb,  $[\text{SO}_4^{2-}]_T$  increases by a factor of 4.4 in the given simulation condition. The effect of the concentration of  $\text{SO}_2$  on  $[\text{SO}_4^{2-}]_T$  has been discussed in Sect. 4.1 above. Figure 5(e) shows the sensitivity of  $[\text{SO}_4^{2-}]_T$  to the ATD loading (100, 200, and 400  $\mu\text{g m}^{-3}$ ). With the increasing of dust loading, the contribution of  $[\text{SO}_4^{2-}]_{\text{photo}}$  to  $[\text{SO}_4^{2-}]_T$  also increases. Figure 5(f) illustrates how sulfate formation is suppressed by different  $\text{NO}_x$  levels (also see Sect. 3.3.2).

The inorganic thermodynamic model (E-AIM II) was employed to estimate  $[\text{H}^+]$  and the liquid water content ( $M_{\text{in,water}}$ ) for the  $\text{SO}_4^{2-}\text{-NH}_4^+\text{-H}_2\text{O}$  system (excluding  $\text{SO}_4^{2-}(\text{d\_salt})$  in reaction 13 of Table 3: dust phase) (Eq. (8)) in both inorganic-salt seeded aqueous phase and dust phase chemistry. The uncertainty in  $M_{\text{in,water}}$  and  $[\text{H}^+]$  influences the partitioning tracers and consequently cause the uncertainty of  $[\text{SO}_4^{2-}]_T$ . The uncertainties in the prediction of  $[\text{H}^+]$  using inorganic thermodynamic models are large because of the limited data (Clegg et al., 1998; Wexler and Clegg, 2002). In this study,  $[\text{H}^+]$  is estimated by E-AIM II (Clegg et al., 1998; Wexler and Clegg, 2002; Clegg and Wexler, 2011) and corrected for the ammonia rich condition (Li et al., 2015; Li and Jang, 2012). The reported uncertainty of  $[\text{H}^+]$  associated with the C-RUV method is  $\pm 18\%$ . Figure S7 illustrates the uncertainties of the major model parameters ( $[\text{H}^+]$ ,  $F_{\text{water}}$ ,  $K_{\text{d,SO}_2}$ ,  $k_{\text{auto}}$  and  $k_{\text{OH,O}_2}$ ) and the prediction of  $[\text{SO}_4^{2-}]_T$ . The uncertainty of  $F_{\text{water}}$  ranges from -20% to 30% due to the uncertainty of the measurement of sulfate ( $\pm 10\%$ ) and ammonia ions ( $\pm 10\%$ ) using PILS-IC. The propagation error in Eqs. (6) and (7) is used to estimate the uncertainty of  $K_{\text{d,SO}_2}$  (-20% to 30%). The uncertainty of  $k_{\text{auto}}$  (-48% to 42%) and  $k_{\text{OH,O}_2}$  (-20% to 22%) are estimated by simulating  $[\text{SO}_4^{2-}]_T$  within the uncertainty of  $K_{\text{d,SO}_2}$  and the measurement of sulfate ( $\pm 10\%$ ). The uncertainty of  $[\text{SO}_4^{2-}]_T$  was estimated to be  $\pm 12\%$  at the end of the simulation. The dust surface area in AMAR is calculated using the geometric surface area. To extend the AMAR model to other dust materials, the molecular level surface area (BET surface area) should be considered in the future. Figure S7 illustrates the influence of the uncertainties in the major model parameters on the prediction of  $[\text{SO}_4^{2-}]_T$ . The uncertainty in  $K_{\text{a,SO}_2}$  ( $\pm 16\%$ ) of  $\text{SO}_2$  was determined using a value from the literature (Adams et al., 2005). The variation in  $[\text{SO}_4^{2-}]_T$  due to the uncertainty in



~~$K_{d,SO_2}$~~  is as small as  $\pm 2\%$ . The reaction rate constants of dust chemistry in the model (Table 3) were semi-empirically determined using preexisting indoor chamber data (Park and Jang, 2016) and chamber characterization. The uncertainty in rate constants associated with observed sulfate concentrations is about  $\pm 10\%$ . Fig. S7 also shows the variation in  $[SO_4^{2-}]_T$  due to the uncertainty in both the reaction of  $SO_2$  with dust surface OH radicals ( $k_{photo}$ ) and the production rate constant of dust surface OH radicals ( $k_{OH,O_2}$ ). Among  $K_{d,SO_2}$ ,  $k_{photo}$ , and  $k_{OH,O_2}$ , the highest uncertainty appears in  ~~$k_{OH,O_2}$~~ .

## 6 Conclusion and atmospheric implication

The AMAR model of this study was developed to predict the oxidation of  $SO_2$  and  $NO_x$  using comprehensive kinetic mechanisms in the gas phase, inorganic seeded aqueous phase and dust phase. The thermodynamic parameters engaged in the partitioning process between gas, inorganic salted aqueous aerosol and dust phases were obtained from known data in the literature (Table 3), and the kinetic parameters for dust chemistry were estimated using previously reported indoor chamber data (Park and Jang, 2016). Overall, the AMAR simulations were consistent with experimentally observed outdoor chamber data (Fig. 3 and Fig. 4) under ambient sunlight. As discussed in the sensitivity analysis (Sect. 5), both the  $[SO_4^{2-}]_T$  and the relative distribution of mechanism-based sulfate formation are sensitive to all major variables (model inputs) including temperature, humidity, sunlight intensity, the quantity of dust loading, and concentrations of  $NO_x$  and  $SO_2$ .

In order to assess the importance of dust chemistry in ambient conditions, the prediction of sulfate formation in the presence of ATD dust needs to be extended to 24-hour simulations under various environmental conditions. Figure S8 shows the output simulated for 24 hours with  $200 \mu g m^{-3}$  of ATD particle loading under urban ( $40 ppb NO_x$ ;  $VOC/NO_x < 5$ ;  $20 ppb SO_2$ ) and rural atmospheres ( $5 ppb NO_x$ ;  $VOC/NO_x > 20$ ;  $2 ppb SO_2$ ). At nighttime, when the temperature drops and humidity increases (70–90%, Fig. S6), the contribution of  $[SO_4^{2-}]_{auto}$  to  $[SO_4^{2-}]_T$  becomes larger than the typical chamber simulation during the daytime. In a rural environment,  $[SO_4^{2-}]_{photo}$  is still the most influential on sulfate formation (0.76 fraction of  $[SO_4^{2-}]_T$  in Fig. S8(a)). For the simulation in a polluted area (Fig. S8(b)), the fraction of  $[SO_4^{2-}]_{photo}$  to  $[SO_4^{2-}]_T$  significantly decreases (0.61) because of the suppression induced by  $NO_x$  (Sect. 3.3.2), but the fraction of  $[SO_4^{2-}]_{auto}$

$[\text{SO}_4^{2-}]_{\text{auto}}$  to  $[\text{SO}_4^{2-}]_{\text{T}}$  increases (0.28). With decreasing sunlight intensity (after 5 PM), Fig. S8 shows the rapid increases in  $[\text{SO}_4^{2-}]_{\text{auto}}$  due to the reaction of dust-phase  $\text{SO}_2$  with ozone, which is the result of daytime photooxidation (Sect. 3.3.1). Fig. S8 suggests that the failure to predict sulfate formation without accurate dust chemistry ( $[\text{SO}_4^{2-}]_{\text{auto}} + [\text{SO}_4^{2-}]_{\text{photo}}$ ) can lead to substantial underestimation of the quantity of total sulfate at regional or global scales.  $\text{SO}_2$  autoxidation alone may partially improve the prediction of sulfate in the presence of mineral dust, but sulfate production can still be largely underestimated and incorrectly predicted in time series when heterogeneous photocatalytic reactions in kinetic mechanisms are not considered.

The ATD particles in this study have chemical and physical properties different from ambient mineral dust particles. In general, the uptake coefficient of  $\text{SO}_2$  in authentic mineral dust particles (e.g. Gobi Desert dust and Saharan dust) is known to be higher than that of ATD particles (Crowley et al., 2010). Thus, the effect of ambient dust particles on heterogeneous photocatalytic oxidation would be much more important than that of the ATD particles of this study. To extend the AMAR model to the prediction of sulfate in the presence of ambient dust particles, the model parameters related to rate constants, partitioning process, and the physical characteristics (e.g. surface area) of dust particles need to be updated with chamber data. In addition to reactions of inorganic species, the influence of organic species (i.e.,  $\text{HCOOH}$ ,  $\text{HCHO}$ , and  $\text{CH}_3\text{CHO}$ ) on dust heterogeneous chemistry needs to be investigated in the future.

## Acknowledgments

This work was supported by grants from the National Institute of Metrological Science (NIMS–2016–3100), the Ministry of Science, ICT, and Future Planning at South Korea (2014M3C8A5032316) and the Fulbright Scholar (from USA to Mongolia).

## Reference

- Adams, J. W., Rodriguez, D., and Cox, R. A.: The uptake of SO<sub>2</sub> on Saharan dust: a flow tube study, *Atmos Chem Phys*, 5, 2679-2689, 2005.
- Atkinson, R., Baulch, D., Cox, R., Hampson Jr, R., Kerr, J., Rossi, M., and Troe, J.: Evaluated kinetic and photochemical data for atmospheric chemistry: supplement VI. IUPAC subcommittee on gas kinetic data evaluation for atmospheric chemistry, *Journal of Physical and Chemical Reference Data*, 26, 1329-1499, 1997.
- Beardsley, R. L., and Jang, M.: Simulating the SOA formation of isoprene from partitioning and aerosol phase reactions in the presence of inorganics, *Atmos Chem Phys*, 16, 5993-6009, 2016.
- Becker, K. H., Kleffmann, J., Kurtenbach, R., and Wiesen, P.: Solubility of nitrous acid (HONO) in sulfuric acid solutions, *The Journal of Physical Chemistry*, 100, 14984-14990, 1996.
- Binkowski, F. S., and Roselle, S. J.: Models-3 Community Multiscale Air Quality (CMAQ) model aerosol component 1. Model description, *Journal of geophysical research: Atmospheres*, 108, 2003.
- Bond, T. C.: Spectral dependence of visible light absorption by carbonaceous particles emitted from coal combustion, *Geophys Res Lett*, 28, 4075-4078, Doi 10.1029/2001gl013652, 2001.
- Bongartz, A., Kames, J., Welter, F., and Schurath, U.: Near-UV absorption cross sections and trans/cis equilibrium of nitrous acid, *The Journal of Physical Chemistry*, 95, 1076-1082, 1991.
- Byun, D., and Schere, K. L.: Review of the governing equations, computational algorithms, and other components of the models-3 Community Multiscale Air Quality (CMAQ) modeling system, *Appl Mech Rev*, 59, 51-77, 10.1115/1.2128636, 2006.
- Chameides, W. L.: The photochemistry of a remote marine stratiform cloud, *Journal of Geophysical Research: Atmospheres*, 89, 4739-4755, 1984.
- Chang, R. Y. W., Sullivan, R. C., and Abbatt, J. P. D.: Initial uptake of ozone on Saharan dust at atmospheric relative humidities, *Geophys Res Lett*, 32, Artn L14815 10.1029/2005gl023317, 2005.
- Chen, H. H., Nanayakkara, C. E., and Grassian, V. H.: Titanium Dioxide Photocatalysis in Atmospheric Chemistry, *Chem Rev*, 112, 5919-5948, 10.1021/cr3002092, 2012.
- Clegg, S., and Wexler, A. S.: Densities and Apparent Molar Volumes of Atmospherically Important Electrolyte Solutions. 2. The Systems H<sup>+</sup>-HSO<sub>4</sub><sup>-</sup>-SO<sub>4</sub><sup>2-</sup>-H<sub>2</sub>O from 0 to 3 mol kg<sup>-1</sup> as a Function of Temperature and H<sup>+</sup>-NH<sub>4</sub><sup>+</sup>-HSO<sub>4</sub><sup>-</sup>-SO<sub>4</sub><sup>2-</sup>-H<sub>2</sub>O from 0 to 6 mol kg<sup>-1</sup> at 25° C Using a Pitzer Ion Interaction Model, and NH<sub>4</sub>HSO<sub>4</sub>-H<sub>2</sub>O and (NH<sub>4</sub>)<sub>3</sub>H(SO<sub>4</sub>)<sub>2</sub>-H<sub>2</sub>O over the Entire Concentration Range, *The Journal of Physical Chemistry A*, 115, 3461-3474, 2011.
- Clegg, S. L., Brimblecombe, P., and Wexler, A. S.: Thermodynamic model of the system H<sup>+</sup>-NH<sub>4</sub><sup>+</sup>-SO<sub>4</sub><sup>2-</sup>-NO<sub>3</sub><sup>-</sup>-H<sub>2</sub>O at tropospheric temperatures, *The Journal of Physical Chemistry A*, 102, 2137-2154, 1998.
- Colberg, C., Luo, B., Wernli, H., Koop, T., and Peter, T.: A novel model to predict the physical state of atmospheric H<sub>2</sub>SO<sub>4</sub>/NH<sub>3</sub>/H<sub>2</sub>O aerosol particles, *Atmos Chem Phys*, 3, 909-924, 2003.
- Colmenares, J. C., and Luque, R.: Heterogeneous photocatalytic nanomaterials: prospects and challenges in selective transformations of biomass-derived compounds, *Chem Soc Rev*, 43, 765-778, 10.1039/c3cs60262a, 2014.

- Crowley, J. N., Ammann, M., Cox, R. A., Hynes, R. G., Jenkin, M. E., Mellouki, A., Rossi, M. J., Troe, J., and Wallington, T. J.: Evaluated kinetic and photochemical data for atmospheric chemistry: Volume V - heterogeneous reactions on solid substrates, *Atmos Chem Phys*, 10, 9059-9223, 10.5194/acp-10-9059-2010, 2010.
- 5 Cwiertny, D. M., Young, M. A., and Grassian, V. H.: Chemistry and photochemistry of mineral dust aerosol, *Annu Rev Phys Chem*, 59, 27-51, 10.1146/annurev.physchem.59.032607.093630, 2008.
- Dong, X., Fu, J. S., Huang, K., Tong, D., and Zhuang, G.: Model development of dust emission and heterogeneous chemistry within the Community Multiscale Air Quality modeling  
10 system and its application over East Asia, *Atmos. Chem. Phys.*, 16, 8157-8180, 10.5194/acp-16-8157-2016, 2016.
- Dupart, Y., King, S. M., Nekat, B., Nowak, A., Wiedensohler, A., Herrmann, H., David, G., Thomas, B., Miffre, A., Rairoux, P., D'Anna, B., and George, C.: Mineral dust photochemistry induces nucleation events in the presence of SO<sub>2</sub>, *P Natl Acad Sci USA*,  
15 109, 20842-20847, 10.1073/pnas.1212297109, 2012.
- Dupart, Y., Fine, L., D'Anna, B., and George, C.: Heterogeneous uptake of NO<sub>2</sub> on Arizona Test Dust under UV-A irradiation: An aerosol flow tube study, *Aeolian Res*, 15, 45-51, 10.1016/j.aeolia.2013.10.001, 2014.
- Gankanda, A., Coddens, E. M., Zhang, Y., Cwiertny, D. M., and Grassian, V. H.: Sulfate  
20 formation catalyzed by coal fly ash, mineral dust and iron (iii) oxide: variable influence of temperature and light, *Environmental Science: Processes & Impacts*, 18, 1484-1491, 2016.
- Goodman, A. L., Li, P., Usher, C. R., and Grassian, V. H.: Heterogeneous uptake of sulfur dioxide on aluminum and magnesium oxide particles, *J Phys Chem A*, 105, 6109-6120, 10.1021/jp004423z, 2001.
- 25 Hoffmann, M. R., Martin, S. T., Choi, W. Y., and Bahnemann, D. W.: Environmental Applications of Semiconductor Photocatalysis, *Chem Rev*, 95, 69-96, DOI 10.1021/cr00033a004, 1995.
- Hoyle, C. R., Fuchs, C., Jarvinen, E., Saathoff, H., Dias, A., El Haddad, I., Gysel, M., Coburn, S. C., Trostl, J., Bernhammer, A. K., Bianchi, F., Breitenlechner, M., Corbin, J. C., Craven, J.,  
30 Donahue, N. M., Duplissy, J., Ehrhart, S., Frege, C., Gordon, H., Hoppel, N., Heinritzi, M., Kristensen, T. B., Molteni, U., Nichman, L., Pinterich, T., Prevot, A. S. H., Simon, M., Slowik, J. G., Steiner, G., Tome, A., Vogel, A. L., Volkamer, R., Wagner, A. C., Wagner, R., Wexler, A. S., Williamson, C., Winkler, P. M., Yan, C., Amorim, A., Dommen, J., Curtius, J., Gallagher, M. W., Flagan, R. C., Hansel, A., Kirkby, J., Kulmala, M., Mohler,  
35 O., Stratmann, F., Worsnop, D. R., and Baltensperger, U.: Aqueous phase oxidation of sulphur dioxide by ozone in cloud droplets, *Atmos Chem Phys*, 16, 1693-1712, 10.5194/acp-16-1693-2016, 2016.
- Huang, L. B., Zhao, Y., Li, H., and Chen, Z. M.: Kinetics of Heterogeneous Reaction of Sulfur Dioxide on Authentic Mineral Dust: Effects of Relative Humidity and Hydrogen Peroxide,  
40 *Environ Sci Technol*, 49, 10797-10805, 10.1021/acs.est.5b03930, 2015.
- Krueger, B. J., Grassian, V. H., Laskin, A., and Cowin, J. P.: The transformation of solid atmospheric particles into liquid droplets through heterogeneous chemistry: Laboratory insights into the processing of calcium containing mineral dust aerosol in the troposphere, *Geophys Res Lett*, 30, Art1148  
45 10.1029/2002gl016563, 2003.

- Li, J., and Jang, M.: [Aerosol acidity measurement using colorimetry coupled with a reflectance UV-visible spectrometer](#), *Aerosol Sci Tech*, 46, 833-842, 2012.
- Li, J., Jang, M., and Beardsley, R. L.: Dialkylsulfate formation in sulfuric acid-seeded secondary organic aerosol produced using an outdoor chamber under natural sunlight, *Environ Chem*, 5, 2015.
- Li, J. W., and Han, Z. W.: A modeling study of the impact of heterogeneous reactions on mineral aerosol surfaces on tropospheric chemistry over East Asia, *Particuology*, 8, 433-441, 10.1016/j.partic.2010.03.018, 2010.
- Liang, J. Y., and Jacobson, M. Z.: A study of sulfur dioxide oxidation pathways over a range of liquid water contents, pH values, and temperatures, *J Geophys Res-Atmos*, 104, 13749-13769, Doi 10.1029/1999jd900097, 1999.
- Linsebigler, A. L., Lu, G. Q., and Yates, J. T.: Photocatalysis on TiO<sub>2</sub> Surfaces - Principles, Mechanisms, and Selected Results, *Chem Rev*, 95, 735-758, DOI 10.1021/cr00035a013, 1995.
- 15 Liu, C., Ma, Q. X., Liu, Y. C., Ma, J. Z., and He, H.: Synergistic reaction between SO<sub>2</sub> and NO<sub>2</sub> on mineral oxides: a potential formation pathway of sulfate aerosol, *Phys Chem Chem Phys*, 14, 1668-1676, 10.1039/c1cp22217a, 2012.
- Liu, Y., Zhu, T., Zhao, D., and Zhang, Z.: Investigation of the hygroscopic properties of Ca(NO<sub>3</sub>)<sub>2</sub> and internally mixed Ca (NO<sub>3</sub>)<sub>2</sub>/CaCO<sub>3</sub> particles by micro-Raman spectrometry, 20 *Atmos Chem Phys*, 8, 7205-7215, 2008.
- Ma, Q. X., Liu, Y. C., and He, H.: Synergistic effect between NO<sub>2</sub> and SO<sub>2</sub> in their adsorption and reaction on gamma-alumina, *J Phys Chem A*, 112, 6630-6635, 10.1021/jp802025z, 2008.
- Martell, A. E., and Smith, R. M.: *Inorganic complexes*, Plenum Press, 1976.
- 25 McNaught, A. D., and Wilkinson, A.: IUPAC. Compendium of Chemical Terminology, 2<sup>nd</sup> ed. (the "Gold Book"), WileyBlackwell; 2nd Revised edition edition, 1997.
- Michel, A. E., Usher, C. R., and Grassian, V. H.: Reactive uptake of ozone on mineral oxides and mineral dusts, *Atmos Environ*, 37, 3201-3211, 10.1016/S1352-2310(03)00319-4, 2003.
- Nanayakkara, C. E., Pettibone, J., and Grassian, V. H.: Sulfur dioxide adsorption and photooxidation on isotopically-labeled titanium dioxide nanoparticle surfaces: roles of surface hydroxyl groups and adsorbed water in the formation and stability of adsorbed sulfite and sulfate, *Phys Chem Chem Phys*, 14, 6957-6966, 10.1039/c2cp23684b, 2012.
- 30 Navea, J. G., Chen, H. H., Huang, M., Carmichel, G. R., and Grassian, V. H.: A comparative evaluation of water uptake on several mineral dust sources, *Environ Chem*, 7, 162-170, 10.1071/En09122, 2010.
- 35 Park, J., and Jang, M.: Heterogeneous photooxidation of sulfur dioxide in the presence of airborne mineral dust particles, *RSC Advances*, 6, 58617-58627, 2016.
- Reyes-Coronado, D., Rodríguez-Gattorno, G., Espinosa-Pesqueira, M., Cab, C., De Coss, R., and Oskam, G.: Phase-pure TiO<sub>2</sub> nanoparticles: anatase, brookite and rutile, *Nanotechnology*, 40 19, 145605, 2008.
- Saliba, N., Moussa, S., and El Tayyar, G.: Contribution of airborne dust particles to HONO sources, *Atmospheric Chemistry and Physics Discussions*, 14, 4827-4839, 2014.
- Saliba, N. A., and Chamseddine, A.: Uptake of acid pollutants by mineral dust and their effect on aerosol solubility, *Atmos Environ*, 46, 256-263, 10.1016/j.atmosenv.2011.09.074, 2012.
- 45 Sarwar, G., Fahey, K., Kwok, R., Gilliam, R. C., Roselle, S. J., Mathur, R., Xue, J., Yu, J., and Carter, W. P.: Potential impacts of two SO<sub>2</sub> oxidation pathways on regional sulfate

- concentrations: aqueous-phase oxidation by NO<sub>2</sub> and gas-phase oxidation by Stabilized Criegee Intermediates, *Atmos Environ*, 68, 186-197, 2013.
- Sarwar, G., Simon, H., Fahey, K., Mathur, R., Goliff, W. S., and Stockwell, W. R.: Impact of sulfur dioxide oxidation by Stabilized Criegee Intermediate on sulfate, *Atmos Environ*, 85, 204-214, 2014.
- Schwartz, S., and White, W.: Solubility equilibria of the nitrogen oxides and oxyacids in dilute aqueous solution, *Adv. Environ. Sci. Eng.:(United States)*, 4, 1981.
- Schwartz, S. E.: Gas-Phase and Aqueous-Phase Chemistry of HO<sub>2</sub> in Liquid Water Clouds, *J Geophys Res-Atmos*, 89, 1589-1598, DOI 10.1029/JD089iD07p11589, 1984.
- Shang, J., Li, J., and Zhu, T.: Heterogeneous reaction of SO<sub>2</sub> on TiO<sub>2</sub> particles, *Sci China Chem*, 53, 2637-2643, 10.1007/s11426-010-4160-3, 2010.
- Tang, M. J., Cziczo, D. J., and Grassian, V. H.: Interactions of Water with Mineral Dust Aerosol: Water Adsorption, Hygroscopicity, Cloud Condensation, and Ice Nucleation, *Chem Rev*, 116, 4205-4259, 10.1021/acs.chemrev.5b00529, 2016.
- Tang, Y. H., Carmichael, G. R., Kurata, G., Uno, I., Weber, R. J., Song, C. H., Guttikunda, S. K., Woo, J. H., Streets, D. G., Wei, C., Clarke, A. D., Huebert, B., and Anderson, T. L.: Impacts of dust on regional tropospheric chemistry during the ACE-Asia experiment: A model study with observations, *J Geophys Res-Atmos*, 109, Artn D19s21 10.1029/2003jd003806, 2004.
- Thiebaud, J., Thevenet, F., and Fittschen, C.: OH Radicals and H<sub>2</sub>O<sub>2</sub> Molecules in the Gas Phase near to TiO<sub>2</sub> Surfaces, *J Phys Chem C*, 114, 3082-3088, 10.1021/jp9102542, 2010.
- Thompson, T. L., and Yates, J. T.: Surface science studies of the photoactivation of TiO<sub>2</sub> new photochemical processes, *Chem Rev*, 106, 4428-4453, 2006.
- Ullerstam, M., Vogt, R., Langer, S., and Ljungstrom, E.: The kinetics and mechanism of SO<sub>2</sub> oxidation by O<sub>3</sub> on mineral dust, *Phys Chem Chem Phys*, 4, 4694-4699, 10.1039/b203529b, 2002.
- Underwood, G. M., Song, C. H., Phadnis, M., Carmichael, G. R., and Grassian, V. H.: Heterogeneous reactions of NO<sub>2</sub> and HNO<sub>3</sub> on oxides and mineral dust: A combined laboratory and modeling study, *J Geophys Res-Atmos*, 106, 18055-18066, Doi 10.1029/2000jd900552, 2001.
- Usher, C. R., Al-Hosney, H., Carlos-Cuellar, S., and Grassian, V. H.: A laboratory study of the heterogeneous uptake and oxidation of sulfur dioxide on mineral dust particles, *J Geophys Res-Atmos*, 107, Artn 4713 10.1029/2002jd002051, 2002.
- Usher, C. R., Michel, A. E., Stec, D., and Grassian, V. H.: Laboratory studies of ozone uptake on processed mineral dust, *Atmos Environ*, 37, 5337-5347, 10.1016/j.atmosenv.2003.09.014, 2003.
- Vlasenko, A., Sjogren, S., Weingartner, E., Stemmler, K., Gaggeler, H. W., and Ammann, M.: Effect of humidity on nitric acid uptake to mineral dust aerosol particles, *Atmos Chem Phys*, 6, 2147-2160, 2006.
- Wagner, C., Schuster, G., and Crowley, J.: An aerosol flow tube study of the interaction of N<sub>2</sub>O<sub>5</sub> with calcite, Arizona dust and quartz, *Atmos Environ*, 43, 5001-5008, 2009.
- Wagner, R., Ajtai, T., Kandler, K., Lieke, K., Linke, C., Muller, T., Schnaiter, M., and Vragel, M.: Complex refractive indices of Saharan dust samples at visible and near UV wavelengths: a laboratory study, *Atmos Chem Phys*, 12, 2491-2512, 10.5194/acp-12-2491-2012, 2012.

- Wexler, A. S., and Clegg, S. L.: Atmospheric aerosol models for systems including the ions  $\text{H}^+$ ,  $\text{NH}_4^+$ ,  $\text{Na}^+$ ,  $\text{SO}_4^{2-}$ ,  $\text{NO}_3^-$ ,  $\text{Cl}^-$ ,  $\text{Br}^-$ , and  $\text{H}_2\text{O}$ , *Journal of Geophysical Research: Atmospheres*, 107, 2002.
- 5 Zhang, X. Y., Zhuang, G. S., Chen, J. M., Wang, Y., Wang, X., An, Z. S., and Zhang, P.: Heterogeneous reactions of sulfur dioxide on typical mineral particles, *J Phys Chem B*, 110, 12588-12596, 10.1021/jp0617773, 2006.
- Zhang, Y.-H., and Chan, C. K.: Understanding the hygroscopic properties of supersaturated droplets of metal and ammonium sulfate solutions using Raman spectroscopy, *The Journal of Physical Chemistry A*, 106, 285-292, 2002.
- 10 Zhong, M., and Jang, M.: Light absorption coefficient measurement of SOA using a UV-Visible spectrometer connected with an integrating sphere, *Atmos Environ*, 45, 4263-4271, 10.1016/j.atmosenv.2011.04.082, 2011.
- Zuend, A., Marcolli, C., Booth, A., Lienhard, D., Soonsin, V., Krieger, U., Topping, D., McFiggans, G., Peter, T., and Seinfeld, J.: New and extended parameterization of the thermodynamic model AIOMFAC: calculation of activity coefficients for organic-inorganic mixtures containing carboxyl, hydroxyl, carbonyl, ether, ester, alkenyl, alkyl, and aromatic functional groups, *Atmos Chem Phys*, 11, 9155-9206, 2011.
- 15

**Table 1. Experiment conditions and simulation results for SO<sub>2</sub> heterogeneous photooxidation on the surface of ATD particles at variety condition of humidity (RH), light sources and initial concentration of traces using indoor chamber data.**

Exp. No. <sup>a</sup>	UV	RH <sup>b</sup> (%)	Temp. <sup>b</sup> (K)	Initial Concentration				Duration <sup>c</sup> (min)	Exp. [SO <sub>4</sub> <sup>2-</sup> ] <sub>T</sub> <sup>f</sup> (μg m <sup>-3</sup> )	Note <sup>g</sup>
				ATD dust <sup>c</sup> (μg m <sup>-3</sup> )	SO <sub>2</sub> <sup>d</sup> (ppb)	NO/NO <sub>2</sub> <sup>d</sup> (ppb)	O <sub>3</sub> <sup>d</sup> (ppb)			
D1	Off	21.0	295.9	295	267	N.A.	N.A.	150	0.61±0.02	<i>K<sub>d,SO<sub>2</sub></sub></i>
D2	Off	55.3	295.0	406	152	0.1/0.6	1.86	148	1.02±0.01	<i>k<sub>auto</sub></i>
D3	Off	80.1	294.5	278	147	0.9/1.6	0.29	147	1.59±0.02	
L1	On	20.4	297.0	123	87.8	0.3/1.7	0.30	120	1.66±0.04	<i>k<sub>OH,SO<sub>2</sub></sub></i>
L2	On	55.2	299.3	120	82.3	0.2/1.9	1.79	120	2.54±0.21	<i>k<sub>auto</sub></i>
L3	On	80.7	298.7	131	78.0	0.2/0.4	0.28	120	5.22±0.19	
L4	On	21.0	296.9	130	78.1	0.1/1.35	64.8	120	4.48±0.14	<i>k<sub>OH,SO<sub>2</sub></sub></i>
D4	Off	20.4	296.6	293	101.0	0.7/1.9	65.4	60	0.158±0.01	<i>k<sub>auto,O<sub>3</sub></sub></i>

<sup>a</sup> “D” denotes experiments under dark condition. “L” denotes experiments with UV light. The dataset D1–D3 and L1–L4 were obtained from the recent laboratory data reported by Park and Jang (2016). Dataset D4 was newly added here to estimate the kinetic parameter of heterogeneous autooxidation of SO<sub>2</sub> in the presence of ozone.

<sup>b</sup> The accuracy of RH is ±5%. The accuracy of temperature is ±0.5 K.

<sup>c</sup> The mass concentration of ATD particles were calculated combining SMPS data, OPC data, the density of dust particles (2.65 g cm<sup>-3</sup>), and the particle size distribution (<3μm). The errors associated with the dust particle mass concentration were ±6%.

<sup>d</sup> The errors associated with the observation of SO<sub>2</sub>, NO, NO<sub>2</sub>, and O<sub>3</sub> were ±0.9%, ±12.5%, ±6.9%, and ±0.2%, respectively.

<sup>e</sup> The duration is the simulation time from the beginning of the experiment to the end of the experiment.

<sup>f</sup> Sulfate concentrations were measured at the end of experiments using PILS–IC. The measurements were not corrected for the particle loss rate to the wall but corrected for the indigenous sulfate from dust particles.

<sup>g</sup> The experiments are noted with the associated kinetic parameters that were empirically determined.

Inserted Cells



**Table 2. Outdoor chamber experiment condition for SO<sub>2</sub> heterogeneously photooxidation on the ATD particles at variety initial concentration of SO<sub>2</sub>, dust particle, and NO<sub>2</sub>.**

Exp. Date	Purpose	RH <sup>a</sup> (%)	Temp. <sup>a</sup> (K)	simulation Time (EST)	Initial Concentration <sup>b</sup>			
					ATD dust <sup>c</sup> ( $\mu\text{g m}^{-3}$ )	SO <sub>2</sub> (ppb)	NO/NO <sub>2</sub> (ppb)	O <sub>3</sub> (ppb)
28/3/2015	SO <sub>2</sub>	18–67	277.1–301.9	11:10–16:30	N.A.	60.1	0.1/0.9	6.3
	SO <sub>2</sub> & dust	24–71	277.8–301.5	10:50–16:30	290.1	56.4	0.1/0.7	0.7
16/6/2015	Low dust	15–49	286.7–313.0	8:40–15:30	90.1	100.0	0.1/0.7	0.7
	High dust	16–48	287.0–311.5	9:30–15:30	403.7	120.1	1.1/1.0	5
12/11/2015	Low SO <sub>2</sub>	24–71	277.8–301.5	8:40–17:30	239.2	119.0	0.5/2.0	3.0
	High SO <sub>2</sub>	14–42	296.2–325.0	9:00–17:30	229.0	271.6	0.2/2.1	2.6
14/4/2017	NO <sub>x</sub> effect	33–95	287.8–314.3	6:30–17:30	496.2	88.1	88.9/13.5	3.0
25/4/2017–1	NO <sub>x</sub> effect	18–89	283.8–313.6	6:00–16:00	414.0	15.0	112.0/13.2	2.2
25/4/2017–2	NO <sub>x</sub> effect	26–94	284.1–312.7	6:00–16:00	478.7	17.5	35.9/3.6	1.9

<sup>a</sup> The accuracy of RH is  $\pm 5\%$ . The accuracy of temperature is  $\pm 0.5$  K.

<sup>b</sup> The errors associated with the observation of SO<sub>2</sub>, NO, NO<sub>2</sub>, O<sub>3</sub>, NH<sub>4</sub><sup>+</sup> and the concentration of dust particle mass were  $\pm 0.9\%$ ,  $\pm 12.5\%$ ,  $\pm 6.9\%$ ,  $\pm 0.2\%$ ,  $5.0\pm\%$  and  $\pm 6\%$ , respectively. The detailed observations of the chemical species during the experiments were shown in Fig. S4 and Fig. S5 in Supporting Information.

<sup>c</sup> The mass concentration of ATD particles were calculated combining SMPS data, OPC data, the density of dust particles ( $2.65 \text{ g cm}^{-3}$ ), and the particle size distribution ( $<3\mu\text{m}$ ).

**Table 3. Dust-phase heterogeneous reactions and their rate constants in the presence of ATD particles.**

Reaction <sup>a</sup>		Rate constant <sup>b</sup>	Coefficients of rate constants <sup>b</sup>		$K_a$ <sup>c</sup>	Reference <sup>d</sup>	Note <sup>e</sup>
			$k_1$	$k_2$			
Partitioning							
1	SO <sub>2</sub> + Dust → SO <sub>2</sub> (d) + Dust	$k_{ads}$	1×10 <sup>-8</sup>			AR05, HZ15	R7
2	SO <sub>2</sub> (d) → SO <sub>2</sub>	$k_{des}$	1×10 <sup>9</sup>	3100	0.013	AR05, HZ15	R8
3	O <sub>3</sub> + Dust → O <sub>3</sub> (d) + Dust	$k_{ads}$	1×10 <sup>-8</sup>			MU03, US01	
4	O <sub>3</sub> (d) → O <sub>3</sub>	$k_{des}$	3×10 <sup>10</sup>	2700	0	MU03, US01	
5	NO <sub>2</sub> + Dust → NO <sub>2</sub> (d) + Dust	$k_{ads}$	1×10 <sup>-8</sup>			CW84	
6	NO <sub>2</sub> (d) → NO <sub>2</sub>	$k_{des}$	1×10 <sup>10</sup>	2500	0	CW84	
7	HNO <sub>3</sub> + Dust → HNO <sub>3</sub> (d) + Dust	$k_{ads}$	1×10 <sup>-8</sup>			SW81, Sc84	
8	HNO <sub>3</sub> (d) → HNO <sub>3</sub>	$k_{des}$	1×10 <sup>15</sup>	8700	15.4	SW81, Sc84	
9	HONO + Dust → HONO(d) + Dust	$k_{ads}$	1×10 <sup>-8</sup>			BK96	
10	HONO(d) → HONO	$k_{des}$	1×10 <sup>10</sup>	4900	0	BK96	
11	N <sub>2</sub> O <sub>5</sub> + Dust → HNO <sub>3</sub> (d) + Dust	$k_{ads}$	7.3×10 <sup>-3</sup>			WS09	
Dust phase							
1	Dust + $h\nu$ → Dust + e <sub>h</sub>	$k_{e,h}^j$	$j_{[ATD]}$			<a href="#">Sect. 3.2.3</a> <a href="#">estimated</a>	R10
2	e <sub>h</sub> → energy	$k_{recom}$	1×10 <sup>-2</sup>			<a href="#">Sect. 3.2.3</a> <a href="#">estimated</a>	R11
3	e <sub>h</sub> + O <sub>2</sub> → OH(d)	$k_{OH,O_2}$	1×10 <sup>-22</sup>	2.3	<a href="#">RH</a>	<a href="#">Sect. 3.2.3</a> <a href="#">estimated</a>	R12
4	SO <sub>2</sub> (d) → SO <sub>4</sub> <sup>2-</sup> (d)	$k_{auto}$	5×10 <sup>-6</sup>			<a href="#">Sect. 3.2.2</a> <a href="#">estimated</a>	R9
5	SO <sub>2</sub> (d) + OH(d) → SO <sub>4</sub> <sup>2-</sup> (d)	$k_{photo}$	1×10 <sup>-12</sup>			<a href="#">Sect. 3.2.4</a> <a href="#">estimated</a>	R13
6	SO <sub>2</sub> (d) + O <sub>3</sub> (d) → SO <sub>4</sub> <sup>2-</sup> (d) + O <sub>2</sub>	$k_{auto,O_3}$	2×10 <sup>-11</sup>			<a href="#">Sect. 3.3.1</a> <a href="#">estimated</a>	R14
7	e <sub>h</sub> + O <sub>3</sub> (d) → OH(d) + O <sub>2</sub>	$k_{OH,O_3}$	1×10 <sup>-12</sup>			<a href="#">Sect. 3.3.1</a> <a href="#">estimated</a>	R15
8	NO <sub>2</sub> (d) → NO <sub>3</sub> <sup>-</sup> (d)	$k_{auto,NO_2}$	6×10 <sup>-5</sup>			<a href="#">Sect. 3.3.2</a> <a href="#">estimated</a>	R18
9	e <sub>h</sub> + NO <sub>2</sub> (d) → HONO(d)	$k_{e,h,NO_2}$	6×10 <sup>-12</sup>			<a href="#">Sect. 3.3.2</a> <a href="#">estimated</a>	R16
10	HONO(d) + $h\nu$ → OH(d) + NO	$k_{HONO}^j$	$j_{[HONO_{10},OH]}$			BK91, AB97	R17
11	NO <sub>2</sub> (d) + OH(d) → NO <sub>3</sub> <sup>-</sup> (d)	$k_{photo,NO_2}$	1×10 <sup>-10</sup>			<a href="#">Sect. 3.3.2</a> <a href="#">estimated</a>	R19

<sup>a</sup> The unit of the chemical species (except dust) is molecule cm<sup>-3</sup> for both partitioning process and the dust phase chemistry. The unit of the dust for model input is mass concentration (μg m<sup>-3</sup>) and is multiplied by a factor of  $2.45 \times 10^{10}$  for simulation.

<sup>b</sup> The unit of reaction rate constants is s<sup>-1</sup> for the first order reactions and cm<sup>3</sup> molecule<sup>-1</sup> s<sup>-1</sup> for the second order reactions.

$k_{ads}$  is uptake rate constant.  $k_{ads} = k_1 \omega f_{dust,M2S} / 4$ , where  $\omega = \sqrt{8RT/(\pi MW)}$  (m s<sup>-1</sup>) and  $f_{dust,M2S} = 3.066 \times 10^{-6}$  (m<sup>2</sup> μg). R is the ideal gas constant and  $MW$  (g mol<sup>-1</sup>) is the molecule weight of chemical species.

$k_{des}$  is desorption rate constant.  $k_{des} = k_1 \exp\left(-\frac{k_2}{T}\right) / (F_{water}(1 + K_a/[H^+]))$ , where  $F_{water}$  is calculated using Eq. (8). [H<sup>+</sup>] and  $M_{in,water}$  are dynamically calculated based on thermodynamic model (E-AIM II) (Clegg et al., 1998; Wexler and Clegg, 2002; Clegg and Wexler, 2011).

The rate constants ( $k$ ) for dust phase reactions is  $k = k_1 \exp(k_2)$ .

$k_{e,h}^j$  and  $k_{HONO}^j$  are photocatalytic reaction rates. The cross sections and quantum yields of dust are estimated (see Sect. 2.2).

<sup>c</sup> Coefficient  $K_a$  is acid dissociation constant (see  $k_{des}$ ).

<sup>d</sup> The rate constant parameters, which are noted as “this study”, are determined using the simulation of indoor chamber data (Park and Jang, 2016) (see Sect. 3). AB97, Atkinson et al. (1997); AR05, Adams et al. (2005); BK91, Bongartz et al. (1991); BK96,

Becker et al. (1996); CW84, Chameides (1984); HZ15, Huang et al. (2015); MU03, Michel et al. (2003); Sc84, Schwartz (1984); SW81, Schwartz and White (1981); US01, Underwood et al. (2001); WS09, Wagner et al. (2009).  
<sup>c</sup> The reactions are noted with the numbers associated with the reaction in main text.

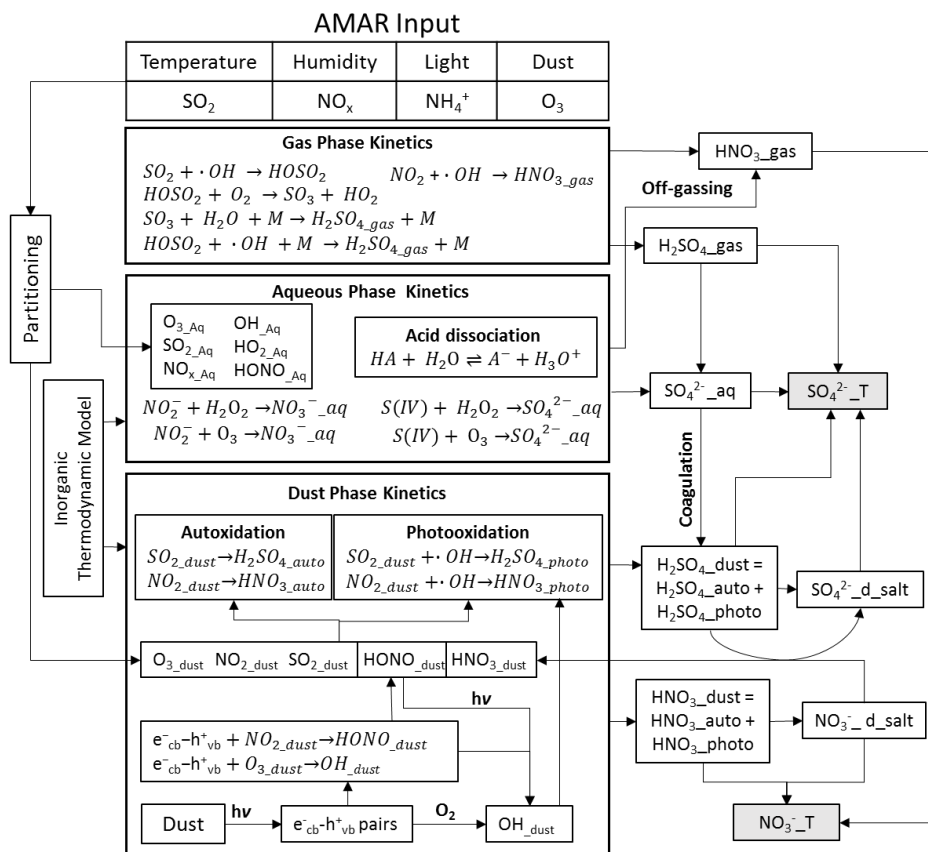


Figure 1. The overall schematic of the AMAR model to simulate heterogeneous SO<sub>2</sub> oxidation. For the description of chemical species, gas phase, aqueous phase and dust phase are symbolized as “gas”, “aq” and “dust”, respectively. SO<sub>4</sub><sup>2-</sup><sub>T</sub>, H<sub>2</sub>SO<sub>4</sub><sub>gas</sub>, SO<sub>4</sub><sup>2-</sup><sub>aq</sub> and H<sub>2</sub>SO<sub>4</sub><sub>dust</sub> are the total sulfate formation and the formation of sulfate from gas phase, aqueous phase and dust phase, respectively. SO<sub>4</sub><sup>2-</sup><sub>d\_salt</sub> and NO<sub>3</sub><sup>-</sup><sub>d\_salt</sub> are the neutralized sulfate and nitrate in dust phase.

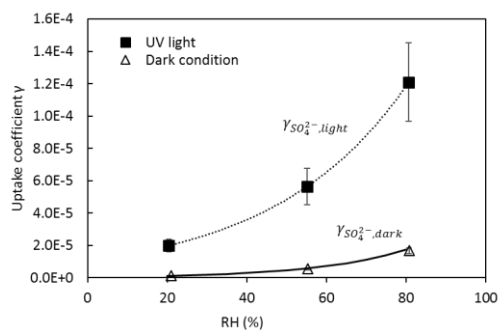
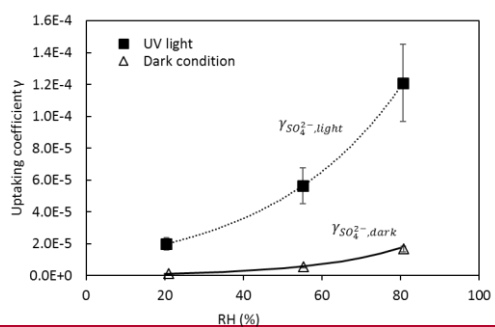


Figure 2. Uptake coefficient ( $\gamma$ ) of  $SO_2$  in the presence of the ATD particles under dark condition and UV light condition. The values of  $\gamma$  were obtained by kinetic model using indoor experimental data. The  $\gamma_{SO_4^{2-},light}$  is correlated to concentration of OH radicals and RH (%). The  $\gamma_{SO_4^{2-},dark}$  is a function of RH. The error bar of  $\gamma$  was derived from the model uncertainty.

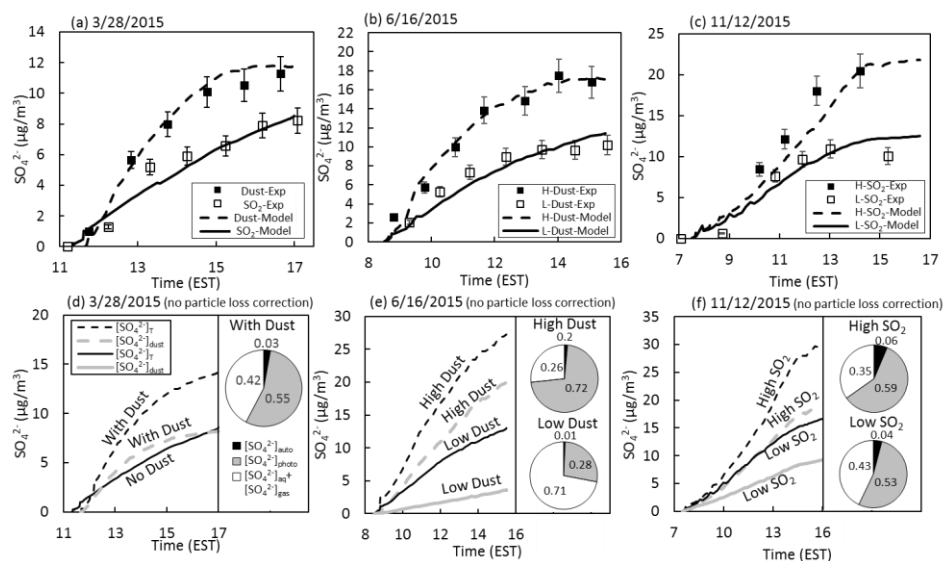


Figure 3. Time profiles of total sulfate concentration ( $\text{SO}_4^{2-}$ ,  $\mu\text{g m}^{-3}$ ) in the UF-APHOR. “Exp” denotes the experimentally observed sulfate ( $[\text{SO}_4^{2-}]_{\text{T}}$ ) and “Model” denotes the model-predicted sulfate. “H” and “L” represent the high and the low initial concentrations of chemical species. The errors associated with the concentration of sulfate is  $\pm 10\%$  originated from the PILS-IC measurement. (a) Sulfate formation with and without ATD particles ( $\text{SO}_2$  60 ppb vs.  $\text{SO}_2$  56 ppb and dust  $290 \mu\text{g m}^{-3}$ ). (b) The high and low loadings of dust particles (dust  $90 \mu\text{g m}^{-3}$  and  $\text{SO}_2$  100 ppb vs. dust  $404 \mu\text{g m}^{-3}$  and  $\text{SO}_2$  120 ppb). (c) The high and the low concentrations of  $\text{SO}_2$  ( $\text{SO}_2$  119 ppb and dust  $239 \mu\text{g m}^{-3}$  vs.  $\text{SO}_2$  272 ppb and dust  $230 \mu\text{g m}^{-3}$ ). For Fig. 3(a), 3(b) and 3(c), the simulations included the chamber dilution and the wall process of gaseous compounds and particles (Sect. S1). For Fig. 3(d), 3(e) and 3(f), the wall process for the particle loss was excluded to estimate the influence of ATD particles on sulfate formation without the chamber artefacts. In Fig. 3(d), 3(e) and 3(f), total sulfate was decoupled into the sulfate originated from dust chemistry ( $[\text{SO}_4^{2-}]_{\text{dust}} = [\text{SO}_4^{2-}]_{\text{photo}} + [\text{SO}_4^{2-}]_{\text{auto}}$ ). The pie charts inserted into Fig. 3(d), 3(e) and 3(f) illustrate how total sulfate is attributed to major pathways at the end of the experiments.

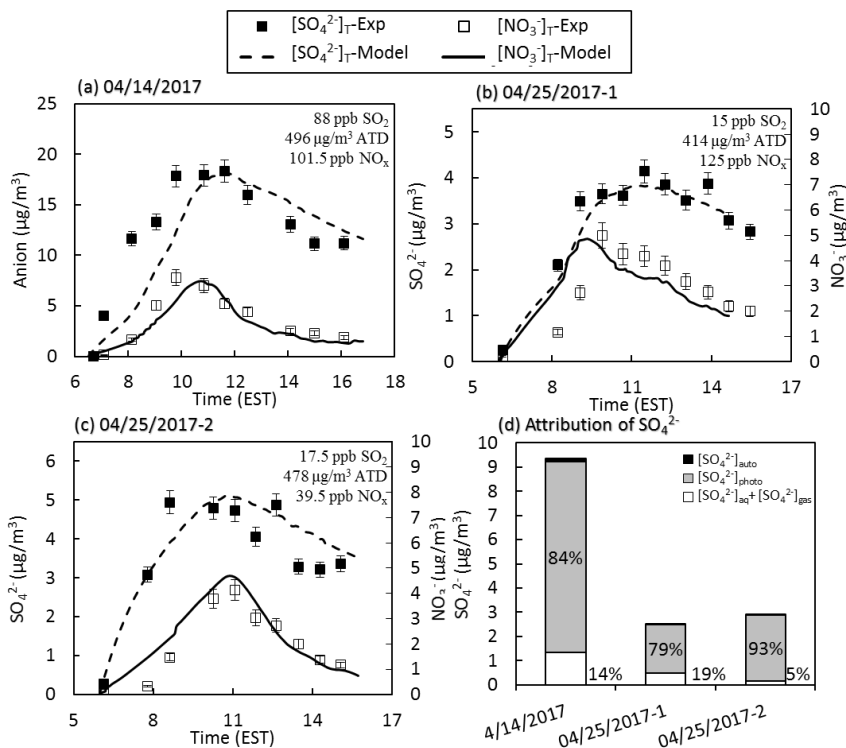


Figure 4. Time profiles of total sulfate concentration ( $[\text{SO}_4^{2-}]_{\text{T}}$ ,  $\mu\text{g}/\text{m}^3$ ) and nitrate concentration ( $[\text{NO}_3^-]_{\text{T}}$ ,  $\mu\text{g}/\text{m}^3$ ) in the dual chamber experiments using UF–APHOR at different  $\text{NO}_x$  levels.

- 5 The concentrations of sulfate and nitrate were measured using PILS–IC during the experiments. The error bars of the concentration of sulfate and nitrate is  $\pm 10\%$  originated from the PILS–IC measurement. The detailed experimental conditions of Fig. 4(a), Fig. 4(b), and Fig. 4(c) are shown in Table 2. Figure 4(d) shows how total sulfate is attributed to aqueous phase reaction (sulfate formation in gas phase + sulfate formation in inorganic salted inorganic aqueous phase) 10 ( $[\text{SO}_4^{2-}]_{\text{aq}} + [\text{SO}_4^{2-}]_{\text{gas}}$ ), dust–phase autooxidation ( $[\text{SO}_4^{2-}]_{\text{auto}}$ ), and dust photochemistry ( $[\text{SO}_4^{2-}]_{\text{photo}}$ ) at the end of the experiments. “Exp” denotes the experimental observation and “Model” denotes the simulation using the AMAR module. The chamber dilution and the wall process of gaseous compounds and particles were included in the simulation (Sect. S1).

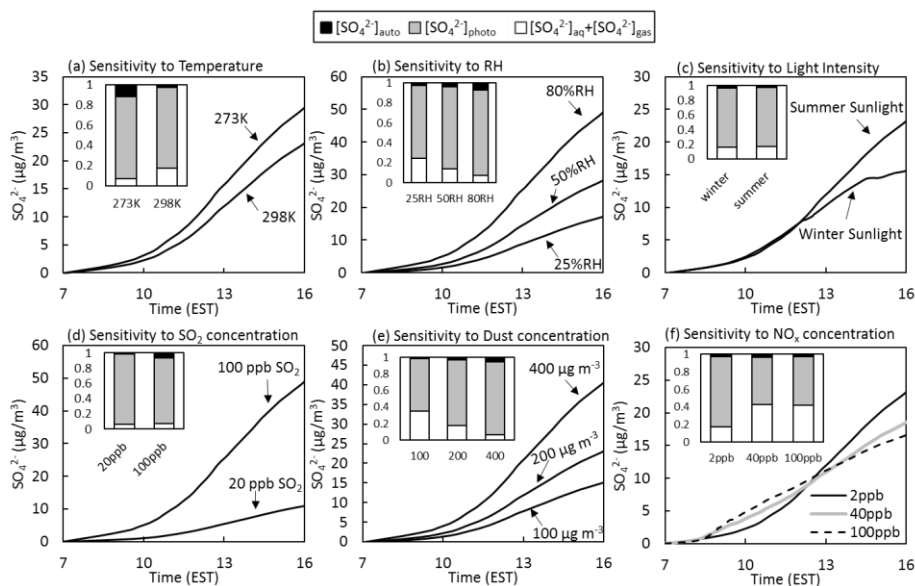


Figure 5. Sensitivity test of AMAR model to (a) temperature at 273K and 298K; (b) RH at 25%, 50% and 80%; (c) sunlight profiles of summertime (25 April, 2017) and wintertime (12 November, 2015) at Gainesville, Florida (latitude/longitude: 29.64185°/-82.347883°); (d) the concentration of SO<sub>2</sub>; (e) the concentration of dust particles; and (f) the NO<sub>x</sub> concentration (initial NO:NO<sub>2</sub>=1:1). The stacked column chart in each figure illustrates how total sulfate is attributed to major pathways at the end of each experiment. For the sensitivity test, the chamber simulation is conducted with 100 ppb of initial SO<sub>2</sub>, 2 ppb of initial NO<sub>2</sub>, 2 ppb of initial O<sub>3</sub> and 200 μg m<sup>-3</sup> of ATD particles at T = 298K and RH = 40% under ambient sunlight on 25 April 2017. NO<sub>x</sub> (rate of flux = 2.7×10<sup>6</sup>, s<sup>-1</sup>) and isoprene (rate of flux = 2.7×10<sup>6</sup>, s<sup>-1</sup>) were constantly added to simulate chamber dilution. The simulation was performed without considering the particle loss to the chamber wall.